

HELSINKI INSTITUTE OF PHYSICS

INTERNAL REPORT

HIP - 2004 - 01

**Looking for Physics Beyond the Standard Model:
Searches for Charged Higgs Bosons at e^+e^- Colliders**

Ari Kiiskinen

Helsinki Institute of Physics
P.O. Box 64, FIN-00014 University of Helsinki, Finland

Dissertation for the degree of Doctor of Science in Technology to be presented with due permission of the Department of Engineering Physics and Mathematics for public examination and debate in Auditorium F1 at Helsinki University of Technology (Espoo, Finland) on the 16th of April, 2004, at 12 o'clock noon.

Helsinki 2004



HELSINKI UNIVERSITY OF TECHNOLOGY P.O. BOX 1000, FIN-02015 HUT http://www.hut.fi		ABSTRACT OF DOCTORAL DISSERTATION	
Author			
Name of the dissertation			
Date of manuscript		Date of the dissertation	
Monograph		Article dissertation (summary + original articles)	
Department			
Laboratory			
Field of research			
Opponent(s)			
Supervisor (Instructor)			
Abstract			
Keywords			
UDC		Number of pages	
ISBN (printed)		ISBN (pdf)	
ISBN (others)		ISSN	
Publisher			
Print distribution			
The dissertation can be read at http://lib.hut.fi/Diss/			

ISBN 952-10-1680-9 (pdf)
ISBN 952-10-1679-5 (print)
ISSN 1455-0563

Helsinki University Press 2004

Acknowledgements

This thesis is based on research work carried out during the years 1998-2003 as a member of the Helsinki Institute of Physics (HIP) group in the DELPHI collaboration. Most of the work has been done at CERN, but the last DELPHI publication and this thesis have been finalised at HIP in Helsinki.

The help and support of a large number of people has been essential for my research work for this thesis. I am most grateful to Professor Risto Orava for giving me the opportunity to work in his group at CERN and for supervising and supporting my work through these years. The contribution of Professor Rainer Salomaa was also important in his role as my thesis supervisor at my home university.

In addition, I would like to thank all the DELPHI collaboration members, without whom the research work presented in this thesis would not have been possible. Most important was the role of Marco Battaglia, from whom I learned the how to do DELPHI physics analysis. Other important people have been all members of the DELPHI charged Higgs team, Pierre Lutz, Tord Ekelöv, Francisco Matorras, Mattias Ellert and Guillermo Gómez-Ceballos. Our team relied a lot on the tools developed by numerous members of all Higgs and WW teams.

I would also like to thank the people at HIP and SEFL in Kumpula for the kind and warm reception I got when migrating from CERN to Kumpula. Special thanks to Professor Dan-Olof Riska, Professor Masud Chaichian and Kenneth Österberg. I have also been very lucky to have always been sharing an office with great colleagues of various nationalities both at CERN and at Kumpula. Thanks to all of them for numerous interesting discussions about various topics.

The financial support of the GRASPANP graduate school program, the Magnus Ehnroot Foundation and the Waldemar von Frenckell Foundation is acknowledged.

The role of all of my many friends in the Finnish and Nordic (either by nationality or by mentality!) communities in Geneva was important to me and made the years I spent in Geneva very special and definitely memorable in many ways. I want to express my gratitude to all of them.

Finally, I want to thank Tea, my parents and my brother with his family for their love and support.

Abstract

This thesis describes direct searches for pair production of charged Higgs bosons performed in the data collected by the DELPHI detector at the LEP collider at CERN. In addition, the possibilities of discovering heavy charged Higgs bosons at possible future high-energy linear colliders are studied.

The existence of charged Higgs bosons is predicted by many extensions of the Standard Model. A possible discovery of these particles would be a solid proof for physics beyond the Standard Model. The discovery of charged Higgs bosons, and measurement of their properties, would also provide useful information about the structure of the more general theory.

New analysis methods were developed for the searches performed at LEP. A large, previously unexplored, mass range was covered but no evidence for the existence of the charged Higgs bosons was found. This allowed the setting of new lower mass limits for the charged Higgs boson within the framework of general two Higgs doublet models. Results have been interpreted and presented in many model hypotheses.

High-energy linear e^+e^- colliders would provide an excellent environment for searches for charged Higgs bosons in future. New analysis methods were developed for the reconstruction and analysis of the decay processes of heavy charged Higgs bosons. The discovery potential and the ability to measure the mass and the decay rates of the charged Higgs boson were demonstrated.

Contents

Introduction	1
Summary of original publications	3
1 The Standard Model	7
1.1 Fermions	7
1.2 Electromagnetic and weak interactions, $SU(2) \times U(1)$ unification	8
1.3 The Higgs mechanism	10
1.4 Quantum Chromo Dynamics (QCD)	12
1.5 Parameters of the Standard Model	12
2 Beyond the Standard Model	14
2.1 Problems of the Standard Model	14
2.2 Grand Unification	15
2.3 Extensions of the Higgs sector	15
2.4 Two Higgs Doublet Models	17
2.5 Production of charged Higgs bosons in e^+e^- collisions	18
2.6 Charged Higgs boson decay modes	20
3 LEP and DELPHI	25
3.1 The LEP collider	25
3.2 The DELPHI detector at LEP	26
3.2.1 Tracking	28
3.2.2 Calorimetry	29
3.2.3 Particle identification	30
3.2.4 Event reconstruction	30

4	Reconstruction methods for hadronic final states	32
4.1	Monte Carlo simulations	32
4.2	Hadronisation	33
4.3	Jet reconstruction and flavour tagging	34
4.4	Mass reconstruction and kinematic fits	35
4.5	Finding the correct quark-antiquark pairs	38
5	Interpretation of the DELPHI H^+H^- search results	40
5.1	The likelihood ratio method for confidence limits	40
5.2	Mass and cross-section limits	42
6	H^+H^- search results of other experiments	46
6.1	Other LEP experiments and the LEP combination	46
6.2	Hadron colliders and indirect searches	46
7	H^+H^- searches in future experiments	49
7.1	The Large Hadron Collider	49
7.2	Linear electron positron colliders	51
8	Conclusions	54
	References	55

Introduction

The creation of the Standard Model during the last decades has been a remarkable success story of modern theoretical and experimental high-energy physics. The model describes, with high precision, all observed elementary particles and their interactions.

The most important unresolved question is considered to be the origin of the mass. In the Standard Model, the masses of fundamental particles result from the interaction of particles with the Higgs field which fills the vacuum. This mechanism can be used to successfully implement the masses of all known particles into the model. However, still today we have no direct experimental evidence which confirms that the origin of the masses really is the Higgs mechanism as the Standard Model describes it. One of the major tasks of the recent, present and coming experimental facilities has been and continues to be to find a definite answer to this question.

The Higgs mechanism of the Standard Model has been constructed by using the principle of maximal simplicity and it contains only the minimal features required to produce the masses for the known particles. Nature, however, does not always follow paths that would appear to be minimalistic. A good example of this is the existence of three generations of fermions. All matter in our universe consists of up and down quarks and electrons. The Standard model has no explanation or reason for the existence of the four additional heavier quarks and two additional charged leptons. There are theories that suggest that this feature, which first appears as an extra complexity of nature, could actually be just the opposite, a natural consequence of a higher level symmetry.

The Higgs mechanism part of the more fundamental model describing nature could also have richer phenomenology than the one predicted by the minimal Standard Model. There are good reasons to believe that the Minimal Standard Model, in the form we have it today, must be replaced at higher energies by another extended theory. There are several candidates for the theory beyond the Standard Model. The extended theories predict the existence of new, up to now unobserved particles including new Higgs states. One of the possibly detectable new Higgs particles is a charged Higgs boson.

Charged Higgs bosons have been searched for in many collider experiments at different energy and mass ranges. No signs of a possible signal have been found so far. Limits for the parameters of the models predicting the existence of charged Higgs bosons have been set as result of searches. The LEP collider at CERN provided large datasets in which charged Higgs bosons could be looked for over a large mass range in direct searches, which is the most model

independent way to exclude the existence of such objects. The searches will continue in future at new colliders with higher collision energies.

The publications presented in this thesis describe experimental searches for charged Higgs bosons at electron-positron-colliders and the development of methods for these analyses. The thesis is organised as follows. Chapter 1 describes the Standard Model of particle physics and the basic concepts of the Higgs mechanism. Chapter 2 discusses extensions of the Standard Model and especially extensions of the Higgs sector, including the Two Higgs Doublet Models, which predict the existence of charged Higgs bosons. Chapter 3 introduces the experimental set up used for a charged Higgs boson search: the LEP collider and the DELPHI detector. Chapter 4 contains more details about phenomenology and analysis methods, which have been used in the DELPHI charged Higgs search analyses, but have not been described in detail in the publications included in this thesis. Chapter 5 presents the statistical methods used to interpret the DELPHI and LEP charged Higgs search results and summarises these results. Chapter 6 lists the results of charged Higgs boson searches performed in other experiments and Chapter 7 draws the conclusions.

Summary of original publications

I *Search for Charged Higgs Bosons at LEP 2*, P. Abreu et al. with A. Kiiskinen (the DELPHI Collaboration), Physics Letters B460 (1999) 484-497.

II *Search for Charged Higgs Bosons and Measurement of $|V_{cs}|$ in quark and lepton flavour-identified events at LEP 2*, A. Kiiskinen on behalf of the DELPHI collaboration, Nuclear Instruments and Methods in Physics Research A 433 (1999) 332-337.

III *Using colour portraits in identifying the quark-antiquark pairs in heavy boson decays*, A. Kiiskinen, V. Nomokonov and R. Orava, DELPHI 98-91 CONF 159 (ICHEP'98 CONF 159) (22 June 1998) HIP 1998-46/EXP.

IV *Search for Charged Higgs Bosons in e^+e^- Collisions at $\sqrt{s} = 189 - 202$ GeV*, J. Abdallah et al. with A. Kiiskinen (the DELPHI Collaboration), Physics Letters B 525 (2002) 17-28.

V *Search for Charged Higgs Bosons at LEP in General Two Higgs Doublet Models*, J. Abdallah et al. with A. Kiiskinen, CERN-EP/2003-064, accepted for publication by Eur. Phys. J. C

VI *Study of $e^+e^- \rightarrow H^+H^-$ at a 800 GeV Linear Collider*, A. Kiiskinen, M. Battaglia and P. Pöyhönen, Physics and experiments with future linear e^+e^- colliders, Editors Adam Para, H. Eugene Fisk, AIP conference proceedings (2001), Vol 578, p. 237. ISBN 0-7354-0017-2.

VII *Pair Production of Charged Higgs Bosons at Future Linear e^+e^- Colliders*, M. Battaglia, A. Ferrari, A. Kiiskinen and T. Mäki, in Proceedings of the Snowmass 2001, the Future of Particle Physics, Snowmass, 2001, edited by Norman Graf, eConf C010630, SLAC-R-599.

Publication I: Search for Charged Higgs Bosons at LEP 2

P. Abreu et al. with A. Kiiskinen (the DELPHI Collaboration)

Physics Letters B460 (1999) 484

Extensions of the Standard Model, such as Super Symmetry (SUSY), contain extensions on the Higgs sector of the models. This results in theories predicting the existence of several physical Higgs bosons such as charged Higgs Bosons (H^+H^-). An experimental search for pair production of H^+H^- in electron positron collisions is performed in the LEP collaborations.

This paper describes the analysis performed with the DELPHI data collected at a collision energy of 183 GeV in 1997. The search results are a combination of independent analyses of the three possible final states: fully hadronic, semileptonic and fully leptonic. The author of this thesis has developed and carried out the analysis of the hadronic decay channel and has been partly responsible for the combination of the results of the different decay channels and for writing the paper.

Publication II: Search for Charged Higgs Bosons and Measurement of $|V_{cs}|$ in quark and lepton flavour-identified events at LEP 2

A. Kiiskinen on behalf of the DELPHI collaboration

Nuclear Instruments and Methods in Physics Research A 433 (1999) 332-337.

Emission of Cherenkov radiation photons from particles that are traversing a medium, with a velocity larger than the speed of light in this medium, can be used for measuring the velocity of the particle. In particle physics experiments, this independent velocity information, combined with the momentum measurement from tracking, is used for defining the particle mass and in this way identifying the particle type. Two physics analyses using the DELPHI Ring Imaging Cherenkov Detector (RICH) are described in this paper. The first one is a search for charged Higgs Bosons and the other is the measurement of the $|V_{cs}|$ element of Cabibbo-Kobayashi-Maskawa mixing matrix.

The author of this thesis has performed the hadronic channel analysis of the charged Higgs search and has written the publication.

Publication III: Using colour portraits in identifying the quark-antiquark pairs in heavy boson decays

A. Kiiskinen, V. Nomokonov and R. Orava

DELPHI 98-91 CONF 159 (ICHEP'98 CONF 159) (22 June 1998) HIP 1998-46/EXP.

In this paper, new methods for identifying the correct quark-antiquark pairs in multiparton events are described. Hadrons in fragmentation are not produced from free quarks or gluons, but from the colour field between them. The kinematics of all final state particles are used

to reconstruct the colour fields between two initial quarks or a quark and a gluon. The reconstructed colour fields are then used to test whether jet pairing has been successful in heavy boson mass reconstruction.

The author of this thesis has been participating in the general development of these methods and has been responsible for applying them to the four jet events such as those resulting from Higgs boson decays.

Publication IV: Search for Charged Higgs Bosons in e^+e^- Collisions at $\sqrt{s} = 189 - 202$ GeV

J. Abdallah et al. with A. Kiiskinen (the DELPHI Collaboration)

Physics Letters B 525 (2002) 17-28

This publication describes the DELPHI charged Higgs search results based on the analyses of the data collected during 1998 and 1999.

The author of this thesis has introduced novel methods for the analysis of the hadronic decay channel and carried out that analysis. He has also been the corresponding author responsible for combining the descriptions of the three analyses into one publication.

Publication V: Search for Charged Higgs Bosons at LEP in general two Higgs doublet models

J. Abdallah et al. with A. Kiiskinen (the DELPHI Collaboration)

CERN-EP/2003-064, accepted for publication by Eur. Phys. J. C

This publication describes the final results of the charged Higgs boson searches using all high energy data collected with the DELPHI detector at LEP.

The author of this thesis has carried out the analysis of the *cscs* decay channel of the charged Higgs boson and contributed to the common systematical error analyses. He has also been one of the two corresponding authors combining results into the form of the final publication.

Publication VI: Study of $e^+e^- \rightarrow H^+H^-$ at a 800 GeV Linear Collider

A. Kiiskinen, M. Battaglia and P. Pöyhönen

Physics and experiments with future linear e^+e^- colliders, Editors Adam Para, H. Eugene Fisk, AIP conference proceedings (2001), Vol 578, p. 237.

This publication studies the possibility of making a full event reconstruction of heavy charged Higgs bosons at the future high energy e^+e^- colliders. It shows for the first time that complete event reconstruction of $H^+H^- \rightarrow t\bar{t}b\bar{b}$ and $H^+H^- \rightarrow W^+h^0W^-h^0$ processes is possible.

It is shown that the mass, the cross-section and decay branching fractions of H^+H^- can be measured. These measurements will provide information about the details of the Higgs mechanism and can therefore be used to discriminate between different models. These results have been also included in the Technical Design Report of the TESLA linear collider.

The author of this thesis has developed the analysis and carried it out with the help of the other authors. He has also written the publication together with the second author.

Publication VII: Pair Production of Charged Higgs Bosons at Future Linear e^+e^- Colliders

M. Battaglia, A. Ferrari, A. Kiiskinen and T. Mäki, in Proceedings of Snowmass 2001, the Future of Particle Physics, Snowmass, 2001, edited by Norman Graf, eConf C010630, SLAC-R-599

This publication describes studies of the potential to discover and measure properties of charged Higgs bosons at future high energy linear colliders, with centre-of-mass energies from 800 GeV to 3 TeV.

The author of this thesis has performed the analyses of the lower energy range, developed analysis methods and tools which have been used in all analyses described in this paper and has been writing large parts of the paper.

Chapter 1

The Standard Model

The Standard Model is a quantum field theory comprising all known elementary constituents of matter and three out of the four known fundamental interactions. The elementary matter particles are leptons and quarks, which both obey the Fermi statistics and are therefore called fermions [1].

The elementary interactions are the strong, weak and electromagnetic interactions and gravity [1],[2]. The interactions are mediated by particles called bosons, (as they obey the Bose statistics): the gluons for strong interactions, W and Z bosons for the weak interactions and photons for the electromagnetic interaction. The only interaction not described by the Standard Model is gravity.

The validity of the Standard Model has been tested in many experiments and its predictions are in strong agreement with the experimental measurements [3],[4].

1.1 Fermions

In the Standard Model, all fermions are placed into left-handed doublets and right-handed singlets. Repeated patterns of doublets and singlets are grouped to form three families or generations. The quark doublets and singlets are [2]

$$\begin{pmatrix} u \\ d \end{pmatrix}_L, \begin{pmatrix} c \\ s \end{pmatrix}_L, \begin{pmatrix} t \\ b \end{pmatrix}_L, d_R, u_R, s_R, c_R, b_R, t_R \quad (1.1)$$

and the lepton doublets and singlets are

$$\begin{pmatrix} \nu_e \\ e^- \end{pmatrix}_L, \begin{pmatrix} \nu_\mu \\ \mu^- \end{pmatrix}_L, \begin{pmatrix} \nu_\tau \\ \tau^- \end{pmatrix}_L, e_R^-, \mu_R^-, \tau_R^-. \quad (1.2)$$

The electric charges and masses of the fermions are [4]

fermion	charge	mass	fermion	charge	mass
d	-1/3	1 to 5 MeV	e^-	-1	511 keV
u	2/3	3 to 9 MeV	ν_e	0	< 3 eV
s	-1/3	75 to 170 MeV	μ^-	-1	105.6 MeV
c	2/3	1.15 to 1.35 GeV	ν_μ	0	< 0.19 MeV
b	-1/3	4.0 to 4.4 GeV	τ^-	-1	1.777 GeV
t	2/3	≈ 174 GeV	ν_τ	0	< 18 MeV

Table 1.1:

where the quoted quark masses are the so called “current-quark masses”. The “constituent masses” of light quarks i.e. their effective masses inside hadrons, would be significantly higher than the current-quark masses.

Charged weak interactions couple the upper members of the $SU(2)_L$ fermion doublets to the lower members in rotated quark doublets of the weak eigenstates [2]

$$\begin{pmatrix} u \\ d' \end{pmatrix}_L, \begin{pmatrix} c \\ s' \end{pmatrix}_L, \begin{pmatrix} t \\ b' \end{pmatrix}_L, \quad (1.3)$$

where the weak eigenstates of the down-type quarks can be defined as linear combinations of the mass eigenstates by using the Cabibbo-Kobayashi-Maskawa (CKM) mixing matrix V_{ij} [5].

$$\begin{pmatrix} d' \\ s' \\ b' \end{pmatrix} = \begin{pmatrix} V_{ud} & V_{us} & V_{ub} \\ V_{cd} & V_{cs} & V_{cb} \\ V_{td} & V_{ts} & V_{tb} \end{pmatrix} \begin{pmatrix} d \\ s \\ b \end{pmatrix} \quad (1.4)$$

The non-diagonal elements of the CKM matrix allow flavour transitions between families. The experimentally measured values of the matrix elements are [5]

$$V_{ij} = \begin{pmatrix} 0.9741 \text{ to } 0.9756 & 0.219 \text{ to } 0.226 & 0.0025 \text{ to } 0.0048 \\ 0.219 \text{ to } 0.226 & 0.9732 \text{ to } 0.9748 & 0.038 \text{ to } 0.044 \\ 0.004 \text{ to } 0.014 & 0.037 \text{ to } 0.044 & 0.9990 \text{ to } 0.9993 \end{pmatrix}. \quad (1.5)$$

1.2 Electromagnetic and weak interactions, $SU(2) \times U(1)$ unification

In the Lagrangian field theory formalism, the equations of motion describing the time evolution of a free fermions are defined by the free fermion Lagrangian [6]

$$\mathcal{L} = \bar{\psi}(i\gamma^\mu \partial_\mu - m)\psi, \quad (1.6)$$

where ψ is the fermion spinor.

The state of a fermion is described by the complex spinor, ψ , but all physical observables must be real i.e. all observables must depend only on $\psi^*\psi$ which is always real as $(x - iy)(x + iy) = x^2 + y^2$. Therefore we can demand that the theory should be invariant under complex phase transitions [6]

$$\psi(\vec{x}, t) \rightarrow \psi'(\vec{x}, t) = e^{-i\chi(\vec{x}, t)}\psi(\vec{x}, t) \quad (1.7)$$

called local gauge transformations, as the transition phase factor χ may depend on the space-time position.

To guarantee that the values of physical measurable quantities do not change in local gauge transformations, the equations of motion must remain unchanged. As the equations of motion are derived from the Lagrangian, their invariance can be ensured if we require that the Lagrangian of the theory must be invariant under these gauge transformations. In other words, we request that our theory exhibits local gauge symmetries.

In the Standard Model, the description of the electromagnetic and weak interactions is derived from the gauge invariance principle by requiring that the Lagrangian remains invariant in local gauge transformations of $U(1)$ and $SU(2)$ symmetry groups.

Our free fermion Lagrangian (1.6) is not invariant under these transformations (1.7) because the transformation of the derivative in the first term of the Lagrangian introduces an extra term, which depends on the derivative of the phase $\partial_\mu\chi(\vec{x}, t)$.

We can, however, modify our Lagrangian and make it gauge invariant by replacing the partial derivative ∂_μ by a new ‘‘covariant derivative’’ of $SU(2) \times U(1)$ transformation [6]

$$D_\mu \equiv \partial_\mu - ig' \frac{Y}{2} B_\mu - ig \frac{\tau_i}{2} W_\mu^i, \quad (1.8)$$

where we have introduced four new gauge fields B_μ and W_μ^i with $i=1,2,3$. The transformation properties of these new gauge fields have been defined to cancel out the $\partial_\mu\chi(\vec{x}, t)$ dependencies in local gauge transformations [6]. Inserting this covariant derivative into the Lagrangian, we get new terms describing interactions between fermions and gauge fields. g and g' are the coupling strengths of these interactions and $\frac{Y}{2}$ and $\frac{\tau_i}{2}$ are the generators of $U(1)$ and $SU(2)$ symmetry transformations.

After a proper normalisation the gauge fields can be written in a form which corresponds to the physical photon and Z^0 boson fields [6]

$$A_\mu = \sin \theta_W W_\mu^{(3)} + \cos \theta_W B_\mu \quad (1.9)$$

$$Z_\mu = \cos \theta_W W_\mu^{(3)} - \sin \theta_W B_\mu. \quad (1.10)$$

where θ_W , called the weak mixing angle or the Weinberg angle and defined as $\sin \theta_W = g' / \sqrt{g^2 + g'^2 Y^2}$ and $\cos \theta_W = g / \sqrt{g^2 + g'^2 Y^2}$, has been used to simplify the coupling constants.

We can also redefine the other two components of the weak fields to correspond to the physical charged weak bosons [6]

$$\begin{aligned} W_\mu^+ &= \sqrt{\frac{1}{2}} \left(W_\mu^{(1)} - iW_\mu^{(2)} \right) \\ W_\mu^- &= \sqrt{\frac{1}{2}} \left(W_\mu^{(1)} + iW_\mu^{(2)} \right). \end{aligned} \tag{1.11}$$

An explicit mass term of form $m^2 W_\mu^i W_i^\mu$ would break the gauge invariance [6] and, therefore, we must assume gauge bosons to be massless. For photon this is in agreement with the experimental observations but for the weak bosons Z and W^\pm this is not correct. We know from experiments that the short range of the weak interaction is due to the large mass of the weak gauge bosons.

1.3 The Higgs mechanism

The problem of implementing the masses of the heavy weak bosons, W^\pm and Z^0 , is solved in the Standard Model by adding a doublet of two complex scalar fields, the Higgs fields ϕ^0 and ϕ^+ , into the theory [2].

$$\phi = \begin{pmatrix} \phi^+ \\ \phi^0 \end{pmatrix} = \sqrt{\frac{1}{2}} \begin{pmatrix} \phi_1 + i\phi_2 \\ \phi_3 + i\phi_4 \end{pmatrix}. \tag{1.12}$$

By using these fields, we define the Higgs potential to be

$$V_{Higgs} = \mu^2 \phi^\dagger \phi + \lambda (\phi^\dagger \phi)^2, \tag{1.13}$$

where the value of λ must be positive to keep the energy of the vacuum bounded from below, but the value of μ^2 can be either positive or negative [2].

If μ^2 were chosen to be positive the potential would have its minimum at $\phi = 0$. Choosing μ^2 to be negative, the minimum of the Higgs potential (1.13) is found at Higgs field values defined by the following condition [2]

$$\phi^\dagger \phi = \frac{1}{2} (\phi_1^2 + \phi_2^2 + \phi_3^2 + \phi_4^2) = \frac{-\mu^2}{2\lambda}. \tag{1.14}$$

To determine the particle spectra by using perturbative expansion, we must expand our potential around a minimum point of the potential. The Higgs potential is symmetric for exchange of the field components ϕ_i and we can choose any minimum point for the location of our vacuum, as no physical quantity can depend on our choice of direction of the coordinate system. As we have to choose one direction to be different from others we break the global $SU(2) \times U(1)$ symmetry [2].

We choose to expand our potential at

$$\phi_1 = \phi_2 = \phi_4 = 0, \quad \phi_3^2 = \frac{-\mu^2}{\lambda} \equiv v^2, \quad (1.15)$$

where we have defined v to be the vacuum expectation value of ϕ_3 . The Higgs field expansion around this chosen vacuum becomes [2]

$$\phi = \sqrt{\frac{1}{2}} \begin{pmatrix} 0 \\ v + h(x) \end{pmatrix}, \quad (1.16)$$

where the value of the Higgs field depends on the function $h(x)$.

We then need to implement the Higgs fields and potentials into our Lagrangian. The kinetic and potential energy terms added to the Lagrangian are [2]

$$\mathcal{L}_{Higgs} = (\partial_\mu \phi)^\dagger (\partial^\mu \phi) - V_{Higgs} = (\partial_\mu \phi)^\dagger (\partial^\mu \phi) - \mu^2 \phi^\dagger \phi - \lambda (\phi^\dagger \phi)^2. \quad (1.17)$$

These new terms in the Lagrangian should also be invariant under our previous local $SU(2) \times U(1)$ gauge transformations. We can, however, directly see that the Higgs field kinetic energy term contains partial derivatives which break the local gauge invariance [6]. We must again replace the partial derivative with the $SU(2) \times U(1)$ covariant derivative (1.8) and we obtain the following $SU(2) \times U(1)$ Higgs Lagrangian

$$\begin{aligned} \mathcal{L}_{Higgs} &= (\partial_\mu + ig' \frac{Y}{2} B_\mu + ig \frac{\tau_i}{2} W_\mu^i) \phi^\dagger (\partial_\mu - ig' \frac{Y}{2} B_\mu - ig \frac{\tau_i}{2} W_\mu^i) \phi \\ &\quad - \mu^2 \phi^\dagger \phi - \lambda (\phi^\dagger \phi)^2 \end{aligned} \quad (1.18)$$

When we substitute the expansion (1.16) around the vacuum expectation value for the Higgs field and use the relation $-\mu^2 = v^2 \lambda$ from (1.15), we get

$$\begin{aligned} \mathcal{L}_{Higgs} &= \frac{1}{2} (\partial_\mu h) (\partial^\mu h) - \frac{1}{4} W_{\mu\nu}^i W_i^{\mu\nu} - \frac{1}{4} B_{\mu\nu} B^{\mu\nu} \\ &\quad + (v+h)^2 \left(\frac{1}{8} g^2 W_\mu^i W_i^\mu + \frac{1}{8} g'^2 B_\mu B^\mu - \frac{1}{4} g g' W_\mu^{(3)} B^\mu \right) \\ &\quad + \frac{1}{2} \lambda v^2 (v+h) - \frac{1}{4} \lambda (v+h)^2. \end{aligned} \quad (1.19)$$

Having a closer look at the second line of (1.19) we can see that there are terms of the order of $v^2 B_\mu B^\mu$, $vh B_\mu B^\mu$ and $h^2 B_\mu B^\mu$ (and similar terms for the W fields). If we compare the form of the $v^2 B_\mu B^\mu$ term to the form of the mass term in our initial free particle Lagrangian (1.6), we can see that they are both of the second order with constant coefficients. These terms in (1.19) can be therefore interpreted as mass terms for the gauge bosons.

$W_\mu^{(3)}$ and B_μ fields, however, can not yet be physical mass eigenstates as there is an extra mixing term for the $W_\mu^{(3)}$ and B_μ fields. We also know that we should have three physical massive bosons (W^+ , W^- and Z^0) and one massless boson (photon). We can achieve this and remove the mixing term and photon mass term by replacing the $W_\mu^{(3)}$ and B_μ fields by A_μ and Z_μ of (1.10).

On the third line of (1.19) we can see that there are also second order mass terms for the Higgs field h which means that the Higgs field has another manifestation as a physical Higgs particle with a mass. The other new terms, with terms mixing Higgs field h and vector boson fields B and W , predict the form of interactions between the Higgs and vector bosons.

By introducing a coupling between the Higgs field and fermions, we can also include the mass terms for fermions. The mass of each fermion is determined by the corresponding Higgs coupling strength.

1.4 Quantum Chromo Dynamics (QCD)

Quarks, and the gluons which bind the quarks together in hadrons, have three colour charges [2]. The existence of colours was postulated to explain the combinatorics of quarks in hadrons, which without a new additional quantum number was violating the Pauli exclusion principle. The existence and number of colour charges has also been experimentally confirmed, for example, in the measurement comparing the hadronic and leptonic decay widths of the Z^0 boson [2].

Analogously to the previous $SU(2)$ weak interaction case, a $SU(3)_C$ symmetry, where C stands for colour, can be used to describe the strong interaction in the Standard Model.

The self-coupling of gluons results in phenomena that are completely different from the behaviour of the electromagnetic and weak interactions. The most striking effect is the fact that the strength of the strong interaction increases with increasing spatial separation. This leads to quark confinement i.e. quarks do not exist as free particles but form colourless compounds of two or three quarks [2].

The non-Abelian nature of QCD and the large value of the strong coupling constant also cause complications for the theory of QCD, as the perturbation theory can not be applied for low energy phenomena and therefore precise quantitative calculations are in many cases not possible [2]. These problems are discussed further in Chapter 4 where the hadronisation process is described. Another complication of QCD was already mentioned at the beginning of this chapter: the definition of the quark masses is not unique, but there are different definitions with values depending on the energy scale [4].

1.5 Parameters of the Standard Model

In the previous sections, we have derived the Lagrangians that describe the different interactions in the Standard Model. The model describes precisely the forms and phenomenology of

interactions but it leaves the values of 18 parameters free. These free parameters are [2]

- The six quark and three lepton masses
- The electroweak coupling constants g and g' and the strong coupling constant α_s
- Three mixing angles and one complex phase in the Cabibbo-Kobayashi-Maskawa quark flavour mixing matrix
- The vacuum expectation value of the Higgs field and the Higgs boson mass (or the Higgs field self-coupling)

The Standard Model has survived all tests and, so far, all its predictions agree with high precision with the experimental results. The only unconfirmed part of the model is the Higgs mechanism. As yet, there is no experimental evidence for the existence of the Higgs boson [5].

Only direct observation of the Higgs boson and precise measurements of its behaviour would confirm that the Higgs mechanism is, indeed, the correct description of the origin of the masses of the weak gauge bosons.

Chapter 2

Beyond the Standard Model

The Standard Model has been extremely successful in describing the experimentally observed particle physics phenomenology up to the electroweak energy scale of the order of 100 GeV. When going to higher energy scales, the Standard Model becomes insufficient and unsatisfactory and a new theory is needed.

2.1 Problems of the Standard Model

The Higgs mechanism of the Standard Model is presently only a hypothesis as no experimental evidence for it has been found. The Higgs mechanism is expected to be proven right or wrong after a few years of operation of the Large Hadron Collider at CERN.

Even if the Higgs mechanism of the Standard Model is proven to be right, the Standard Model gives no answers to many fundamental questions such as the origin of generations, values of the fundamental constants, the equality of the electric charges of proton and positron and the role of gravity [7].

As gravity is not included in it, the Minimal Standard Model can not describe phenomena at the Planck mass energy scale (10^{19} GeV/ c^2) where gravity becomes significant. Furthermore, there is a serious conceptual problem, known as the gauge hierarchy or naturalness problem [8],[7] which suggests that the Minimal Standard Model will already fail much before the Planck scale.

In order to produce masses of the order of 100 GeV/ c^2 for the massive gauge bosons, the Higgs field mass term μ^2 should also be of the order of 100 GeV/ c^2 . The mass of a scalar field is affected by quantum mechanical corrections. Due to the uncertainty principle, virtual particles with arbitrarily high energy can be created in loop diagrams and the contributions of the fermion loop corrections will be of the order of the energy cut off scale of the theory. If the Standard Model were to hold up to the Planck scale i.e. the cut off scale of the Standard Model was the Planck mass scale, the Higgs field mass would be of the order of the Planck mass 10^{19} GeV/ c^2 . The effect of these corrections could be cancelled out if the bare mass of the Higgs field was also of the order of the Planck mass and so finely-tuned that the correction

would exactly cancel out the opposite sign bare mass so that the effective mass would be of the order of $100 \text{ GeV}/c^2$. This would make the theory unstable as a very small variation of any model parameter would cause the whole theory to explode which is not a natural and desired property for a theory.

A good candidate for solving the problem of the fermion loop corrections in the Higgs field mass is the supersymmetry (SUSY). In SUSY, both fermions and bosons are grouped into the fundamental representation and it predicts the existence of new bosonic (fermionic) superpartners for all fermions (bosons). SUSY solves in an elegant way the naturalness problem, as the fermion and boson loop corrections in the Higgs boson mass have opposite signs and cancel each other out naturally [9].

2.2 Grand Unification

The theory of symmetry groups is the basis of the Standard Model. The aim of particle physics is to continue still further and formulate a Grand Unified Theory (GUT) in which the $SU(3)_c$, $SU(2)_W$ and $U(1)_Y$ symmetries of the Standard Model become sub-groups of a larger grand unified group. At sufficiently high energies, all these three interactions would be described by one single coupling constant g_G [2].

In the minimal version of the Standard Model, this unification does not happen as the extrapolations of the three coupling constants do not meet each other at one unique energy, as can be seen in Fig 2.1a. Some new physics phenomena are therefore required between the electroweak energy scale of the Standard Model and the GUT energy scale to modify the evolution of the coupling strengths, so that unification would happen.

There have been many attempts to formulate a Grand Unified Theory and to solve the problems of the Standard Model [9]. The most studied and relatively successful unified theory is the supersymmetric GUT. Fig 2.1b shows how the electroweak and strong coupling constants meet at energy of the order of 10^{16} GeV in a model containing supersymmetric particles.

2.3 Extensions of the Higgs sector

In the minimal version of the Standard Model, there is one Higgs field doublet which is needed to create the masses of the weak gauge bosons and fermions. The Higgs mechanism is, however, a completely theoretical construction implemented into the model to allow gauge invariant mass terms. There is no experimental confirmation for the Higgs mechanism or for the existence of the Higgs boson.

The Standard Model Higgs sector has been chosen to be as simple as possible for the reason of convenience, but nature is not always described best by what would seem to be the minimalistic description. This can be seen for example in the case of fermion generations. The Standard Model would be simpler with only one generation of fermions but in reality there are (at least) two other extra families, where the Model does not predict their existence. In a similar way,

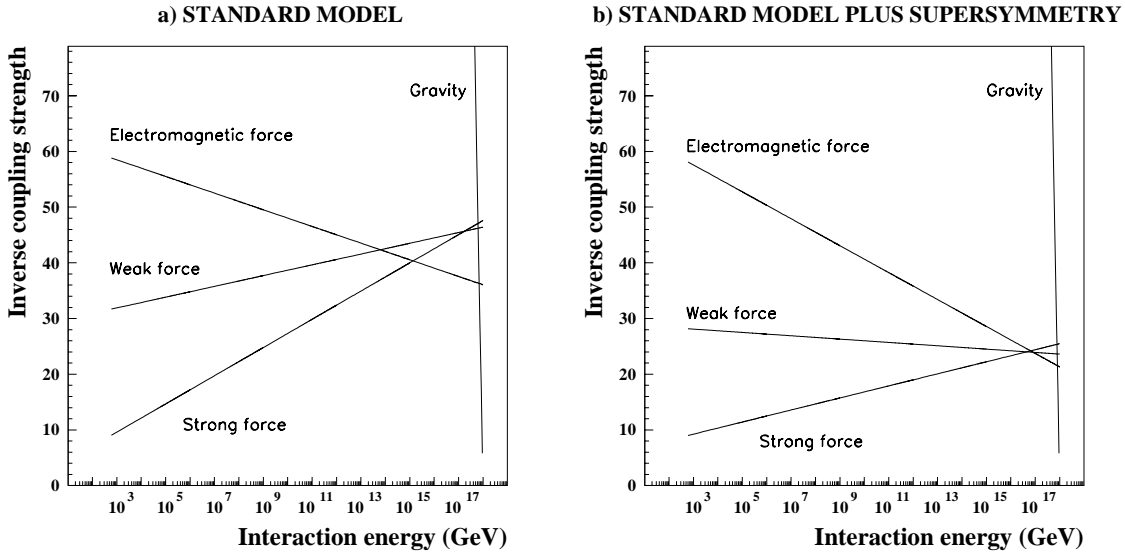


Figure 2.1: Schematic illustration of the energy dependence of the coupling strengths in the Minimal Standard Model and in Supersymmetry. Pictures adopted from [10].

the Higgs sector could also have more fields and particles than the minimum choice in the Standard Model. We can therefore try to extend the contents of the Higgs sector by adding new multiplets of Higgs fields into the theory.

Any extended model must always be in agreement with all experimental data which means that the new model can not predict any new phenomena which are in contradiction with measurements. There are two major constraints [11].

The first experimental requirement is that $\rho = m_W^2 / (m_Z^2 \cos^2 \theta_W)$ is very close to 1. It can be shown that at tree level i.e. without higher order quantum corrections, $\rho = 1$ can be naturally satisfied if the model contains only Higgs singlets or doublets [11].

The other experimental constraint is the absence of flavour changing neutral currents (FCNC). Experiments have excluded the existence of FCNC processes and the Standard Model does not allow them. However, if fermions coupled to two Higgs doublets, Higgs boson mediated FCNC processes would become possible. Their existence could be avoided in two Higgs doublet models by choosing the Higgs boson masses to be very heavy, which is not satisfactory as a light Higgs boson would be needed to produce masses for the weak bosons [11]. A more elegant solution, proposed by Glashow and Weinberg [12], is to apply restrictions to couplings of the Higgs doublets to fermions so that any fermion with a given electric charge couples only to one Higgs doublet.

2.4 Two Higgs Doublet Models

The most straightforward extension of the Standard Model Higgs sector, fulfilling the $\rho = 1$ requirement, is the addition of another complex Higgs field doublet to the model [11]. The result is a Two Higgs Doublet Model (2HDM).

There are alternative options for arranging the Higgs-fermion couplings so that flavour changing neutral currents can be avoided. Two most commonly used choices are called type I and type II [11]. In type I, only one Higgs doublet couples to fermions and in type II, one doublet couples to up-type fermions and the other doublet to down-type fermions.

The Higgs potential with two complex scalar fields ϕ_1 and ϕ_2 is as follows [11]

$$\begin{aligned}
 V(\phi_1, \phi) &= \lambda_1(\phi_1^\dagger\phi_1 - v_1^2)^2 + \lambda_2(\phi_2^\dagger\phi_2 - v_2^2)^2 \\
 &+ \lambda_3[(\phi_1^\dagger\phi_1 - v_1^2) + (\phi_2^\dagger\phi_2 - v_2^2)]^2 \\
 &+ \lambda_4[(\phi_1^\dagger\phi_1)(\phi_2^\dagger\phi_2) - (\phi_1^\dagger\phi_2)(\phi_2^\dagger\phi_1)] \\
 &+ \lambda_5[\text{Re}(\phi_1^\dagger\phi_2) - v_1v_2 \cos \xi]^2 \\
 &+ \lambda_6[\text{Im}(\phi_1^\dagger\phi_2) - v_1v_2 \sin \xi]^2
 \end{aligned} \tag{2.1}$$

where the λ_i are real parameters.

If all λ_i are non-negative the minimum of the potential is

$$\langle \phi_1 \rangle = \begin{pmatrix} 0 \\ v_1 \end{pmatrix}, \langle \phi_2 \rangle = \begin{pmatrix} 0 \\ v_2 e^{i\xi} \end{pmatrix} \tag{2.2}$$

The imaginary phase ξ would allow CP-violation in the Higgs sector, but in most models, such as supersymmetric models, λ_5 and λ_6 are equal and in this case the number of degrees of freedom is decreased and the phase ξ can be rotated away by a redefinition of one of the fields.

The ratio of the vacuum expectation values

$$\tan \beta = v_2/v_1 \tag{2.3}$$

defines the relative contributions of the two doublets in the physical Higgs bosons and their couplings.

This model leads into five physical Higgs bosons [11]. Two of them are neutral CP-even scalars

$$\begin{aligned}
 H^0 &= \sqrt{2}[(\text{Re}(\phi_1^0) - v_1) \cos \alpha + (\text{Re}(\phi_2^0) - v_2) \sin \alpha] \\
 h^0 &= \sqrt{2}[-(\text{Re}(\phi_1^0) - v_1) \sin \alpha + (\text{Re}(\phi_2^0) - v_2) \cos \alpha]
 \end{aligned} \tag{2.4}$$

with masses

$$m_{H^0, h^0}^2 = \frac{1}{2} \left[\mathcal{M}_{11} + \mathcal{M}_{22} \pm \sqrt{(\mathcal{M}_{11} + \mathcal{M}_{22})^2 + 4\mathcal{M}_{12}^2} \right] \quad (2.5)$$

where \mathcal{M}_{ij} are the matrix elements of the mass-squared mixing matrix

$$\mathcal{M} = \begin{pmatrix} 4v_1^2(\lambda_1 + \lambda_3) + v_2^2\lambda_5 & (4\lambda_3 + \lambda_5)v_1v_2 \\ (4\lambda_3 + \lambda_5)v_1v_2 & 4v_2^2(\lambda_2 + \lambda_3) + v_1^2\lambda_5 \end{pmatrix} \quad (2.6)$$

and the mixing angle α is defined as

$$\begin{aligned} \sin 2\alpha &= \frac{2\mathcal{M}_{12}}{\sqrt{(\mathcal{M}_{11} + \mathcal{M}_{22})^2 + 4\mathcal{M}_{12}^2}} \\ \cos 2\alpha &= \frac{\mathcal{M}_{11} - \mathcal{M}_{22}}{\sqrt{(\mathcal{M}_{11} + \mathcal{M}_{22})^2 + 4\mathcal{M}_{12}^2}}, \end{aligned} \quad (2.7)$$

The third Higgs boson is a CP-odd neutral pseudoscalar

$$A^0 = \sqrt{2}[(\text{Im}\phi_1^0 - v_1) \sin \beta + (\text{Im}\phi_2^0 - v_2) \cos \beta] \quad (2.8)$$

with mass

$$m_{A^0}^2 = \lambda_6(v_1^2 + v_2^2). \quad (2.9)$$

The last two Higgs bosons are the two charged scalars

$$H^\pm = -\phi_1^\pm \sin \beta + \phi_2^\pm \cos \beta, \quad (2.10)$$

with mass $m_{H^\pm}^2 = \lambda_4(v_1^2 + v_2^2)$.

2.5 Production of charged Higgs bosons in e^+e^- collisions

Charged Higgs bosons can be pair-produced in e^+e^- annihilations in the s-channel process via virtual photon or Z^0 . The Feynman diagram for the pair-production process of charged Higgs bosons, $e^+e^- \rightarrow H^+H^-$, followed by one of the possible decay processes, $H^+H^- \rightarrow c\bar{s}c\bar{s}$, is shown in Fig. 2.2.

At tree level, the cross-section of the s-channel pair-production process of charged Higgs bosons in e^+e^- annihilation depends only on the mass of the charged Higgs boson and is [13]

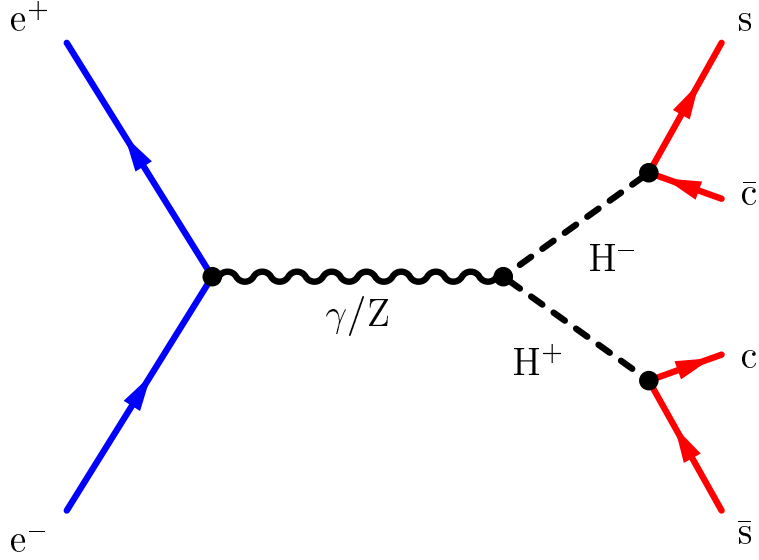


Figure 2.2: Feynman diagram for the $e^+e^- \rightarrow H^+H^- \rightarrow c\bar{c}s\bar{s}$ process.

$$\sigma(e^+e^- \rightarrow H^+H^-) = \frac{2G_F^2 m_W^4 \sin^4 \theta_W}{3\pi s} \left[1 + \frac{2\hat{v}_e \hat{v}_H}{1 - m_Z^2/s} + \frac{(\hat{a}_e^2 + \hat{v}_e^2) \hat{v}_H^2}{(1 - m_Z^2/s)^2} \right] \left(1 - \frac{4m_H^2}{s} \right)^{3/2} \quad (2.11)$$

where

$$\hat{a}_e = \frac{1}{4 \cos \theta_W \sin^2 \theta_W}, \quad \hat{v}_e = \frac{-1 + 4 \sin^2 \theta_W}{4 \cos^2 \theta_W \sin^2 \theta_W}, \quad \hat{v}_H = \frac{-1 + 2 \sin^2 \theta_W}{2 \cos^2 \theta_W \sin^2 \theta_W}.$$

The cross-section of pair-production decreases as a function of increased mass of the charged Higgs boson and vanishes at the kinematical threshold, where the mass of a charged Higgs boson becomes half of the centre-of-mass energy. Publications I-V describe physics analyses performed at the LEP collider which is described in Chapter 3. At LEP, the highest electron-positron collision energies were above 200 GeV, allowing pair-production of charged Higgs bosons up to 100 GeV/ c^2 mass. The 2HDM cross-section for 40-95 GeV/ c^2 charged Higgs bosons at 206.3 GeV centre-of-mass energy can be seen in Fig. 5.3. Publications VI and VII describe studies of the discovery potential for charged Higgs bosons at 800 GeV and 3 TeV linear electron-positron colliders where pair-production of charged Higgs bosons is possible up to masses of 400 GeV/ c^2 and 1.5 TeV/ c^2 .

Within most models and model parameter choices, as discussed in more detail in the following section, the charged Higgs bosons produced in e^+e^- collisions decay into fermions practically immediately at the spot where they are created. Therefore, charged Higgs bosons themselves

are not detected in the particle detectors of the e^+e^- collider experiments, but information about them can be obtained by detecting and studying the long lived particles produced in the decay processes.

The most crucial points in all analyses described in this thesis are the efficient detection of all the decay products of charged Higgs bosons and successful reconstruction of the properties of the measured decay products of charged Higgs bosons. A full chapter of this thesis, Chapter 4, is devoted to methods used for reconstruction of the properties of the charged Higgs bosons in hadronic decay processes such as $e^+e^- \rightarrow H^+H^- \rightarrow c\bar{s}c\bar{s}$ shown in Fig. 2.2.

2.6 Charged Higgs boson decay modes

The interactions of the charged Higgs bosons with fermions are determined by the form of the Lagrangian [14],[15] which is for model type II

$$\begin{aligned} \mathcal{L} = & \frac{g}{\sqrt{2}} \left\{ \left(\frac{m_{Dj}}{M_W} \right) \tan \beta \bar{U}_{L_j} V_{ij} D_{R_i} + \left(\frac{m_{U_i}}{M_W} \right) \cot \beta \bar{U}_{R_i} V_{ij} D_{L_j} \right. \\ & \left. + \left(\frac{m_{l_i}}{M_W} \right) \tan \beta \bar{\nu}_{l_i} l_{R_i} \right\} H^+ + h.c. \end{aligned} \quad (2.12)$$

and for model type I

$$\begin{aligned} \mathcal{L} = & \frac{g}{\sqrt{2}} \left\{ - \left(\frac{m_{Dj}}{M_W} \right) \cot \beta \bar{U}_{L_j} V_{ij} D_{R_i} + \left(\frac{m_{U_i}}{M_W} \right) \cot \beta \bar{U}_{R_i} V_{ij} D_{L_j} \right. \\ & \left. - \left(\frac{m_{l_i}}{M_W} \right) \cot \beta \bar{\nu}_{l_i} l_{R_i} \right\} H^+ + h.c. \end{aligned} \quad (2.13)$$

where R and L stand for right-handed and left-handed helicities, indices i, j are the three flavours of up and down-type quarks and charged leptons (U, D and l) and V_{ij} are the Cabibbo-Kobayashi-Maskawa matrix elements describing the mixing between quark flavours.

The partial decay widths of the charged Higgs boson can be directly calculated from the Lagrangians (2.12) and (2.13). For model type II, the decay widths to quarks and leptons become [11]

$$\Gamma(H^+ \rightarrow U_i \bar{D}_j) = 3 |V_{ij}| \frac{g^2 m_{H^+}}{32\pi m_W^2} (\tan^2 \beta m_{Dj}^2 + \cot^2 \beta m_{U_i}^2) \quad (2.14)$$

$$\Gamma(H^+ \rightarrow l_i^+ \nu_l) = \frac{g^2 m_{H^+}}{32\pi m_W^2} (\tan^2 \beta m_{l_i}^2) \quad (2.15)$$

where the additional factor of 3 in the quark decay widths is the number of colours.

The branching fractions of charged Higgs bosons to different fermion pairs are directly proportional to the decay widths. In the case of the model type II, the ratio of hadronic and leptonic decay rates becomes

$$\frac{Br(H^+ \rightarrow U_i \bar{D}_j)}{Br(H^+ \rightarrow l_i^+ \nu_l)} = \frac{3|V_{ij}|(\tan^2 \beta m_{D_j}^2 + \cot^2 \beta m_{U_i}^2)}{\tan^2 \beta m_{l_i}^2}. \quad (2.16)$$

Substituting the fermion masses and CKM matrix elements, see Table 1.1 and (1.5), into (2.16) we can calculate the relative branching fractions for any fermion pair as a function of $\tan \beta$.

Here we have to note that so far we have only used three level decay widths and for more precise calculations, we have taken into account higher order corrections. The radiative QCD correction for the quark channel decay width is [13]

$$\Gamma(H^+ \rightarrow U_i \bar{D}_j) \Rightarrow \Gamma(H^+ \rightarrow U_i \bar{D}_j) \left[1 + \frac{17}{3} \left(\frac{\alpha_s}{\pi} \right) + O(\alpha_s^2) \right] \quad (2.17)$$

where the value of the strong coupling constant depends on the energy scale and has been measured to have a value of 0.12 at the Z^0 boson mass scale [4]. At mass scale of around 90 GeV/ c^2 , the radiative QCD correction for the quark decay rate is therefore of the order of 20%.

Another dynamic energy dependent effect with a larger impact on the results is the ‘‘running’’ of the quark masses. All the Higgs interaction terms in the Lagrangians above are proportional to effective quark masses at the energy scale of the Higgs boson decay. The effective quark masses at the Higgs boson mass scale are [13]

$$m_q(m_H) = m_q(M_q) \left[\frac{\alpha_s(m_H)}{\alpha_s(M_q)} \right]^{\frac{12}{33-2N_F}} \frac{1 + c_1[\alpha_s(m_H)/\pi] + c_2[\alpha_s(m_H)/\pi]^2}{1 + c_1[\alpha_s(M_q)/\pi] + c_2[\alpha_s(M_q)/\pi]^2} \quad (2.18)$$

where $m_q(M_q)$ are the ‘‘current-quark masses’’ i.e. the effective quark masses in the quarks’ own energy scales $M_q = m_q(M_q)$, which were given in Table 1.1. The values of the coefficients c_1 and c_2 are 1.17 (1.01) and 1.50 (1.39) for b (c) quarks. The effect of quark mass running is as large as the order of a 50% reduction in the value of the c quark mass when going to the energy scale of m_Z from the energy scale of M_c . As the decay widths are proportional to the square of the fermion masses, the running of quark mass results in a reduction factor of the order of 4 in the ratio $Br(H^+ \rightarrow cs)/Br(H^+ \rightarrow \tau\nu)$ between energy scales of the order of a few GeV and 100 GeV.

If the mass of the charged Higgs boson is larger than the t quark mass, making the $H^+ \rightarrow t\bar{b}$ decay kinematically allowed, this decay dominates for any $\tan \beta$ value, as both t and b quarks are significantly heavier than any other quarks or leptons.

For charged Higgs bosons with a mass below the t quark mass, the situation is more complicated as the mass of the τ lepton is larger than the mass of the s quark. The branching ratios

for a charged Higgs boson below the t quark mass in 2HDM type II, with the effect of quark mass running taken into account, are shown in Fig. 2.3

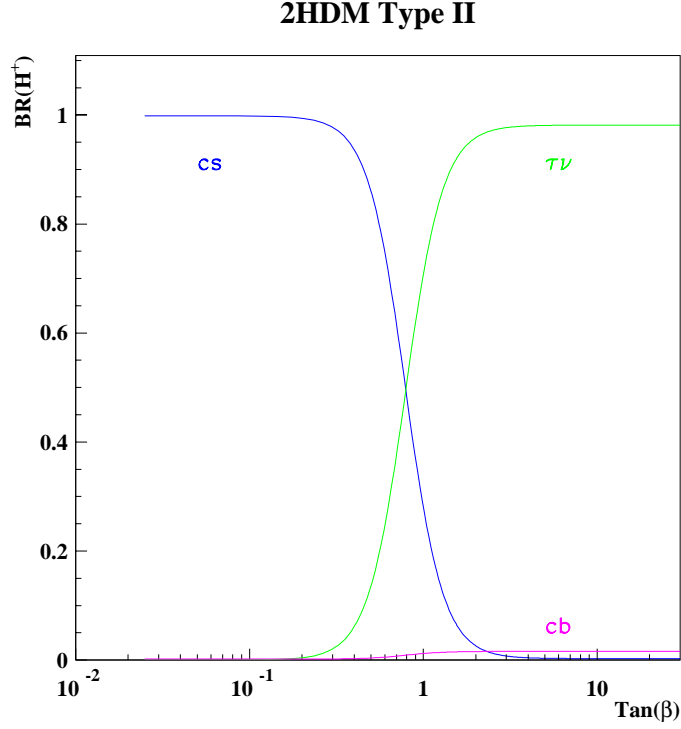


Figure 2.3: Decay branching ratios of the charged Higgs boson in 2HDM type II.

In model type I, the fermionic decay widths are

$$\Gamma(H^+ \rightarrow U_i \bar{D}_j) = 3|V_{ij}| \frac{g^2 m_{H^+}}{32\pi m_W^2} (\cot^2 \beta m_{D_j}^2 + \cot^2 \beta m_{U_i}^2) \quad (2.19)$$

$$\Gamma(H^+ \rightarrow l_i^+ \nu_l) = \frac{g^2 m_{H^+}}{32\pi m_W^2} (\cot^2 \beta m_{l_i}^2). \quad (2.20)$$

where the $\tan \beta$ dependencies cancel each other out and the branching ratios depend only on the fermion masses:

$$\frac{Br(H^+ \rightarrow U_i \bar{D}_j)}{Br(H^+ \rightarrow l_i^+ \nu_l)} = \frac{3|V_{ij}|(m_{D_j}^2 + m_{U_i}^2)}{m_{l_i}^2}. \quad (2.21)$$

In model type I, only one of the doublets has couplings to fermions and the other doublet only couples to bosons. The doublet with fermionic couplings is suppressed at high values of

$\tan\beta$ and this can lead to large bosonic branching fraction if bosonic decays are kinematically allowed. If there is a light neutral Higgs boson, h^0 , the decay process $H^+ \rightarrow W^+h^0$ can be significant compared to $H^+ \rightarrow t\bar{b}$ decay at high values of the mass of the charged Higgs boson [11]. Already at lower mass values, accessible at LEP, decay to W^*A bosons may become significant if there is a light pseudo-scalar Higgs, A .

The partial decay width of the cascade decay involving the virtual W^* boson can be obtained by integrating over the Dalitz plot (over the momenta of final state fermions f and \bar{f}') and it becomes [16]

$$\Gamma(H^+ \rightarrow AW^* \rightarrow Af\bar{f}') = \frac{9g^4 m_{H^+}}{256\pi^3} G_{AW} \quad (2.22)$$

where the function G_{AW} is

$$\begin{aligned} G_{AW} = & \frac{1}{4} \left\{ 2(-1 + \kappa_W - \kappa_A) \sqrt{\lambda_{AW}} \left[\frac{\pi}{2} + \arctan \left(\frac{\kappa_W(1 - \kappa_W + \kappa_A) - \lambda_{AW}}{(1 - \kappa_A) \sqrt{\lambda_{AW}}} \right) \right] \right. \\ & \left. + (\lambda_{AW} - 2\kappa_A) \log(\kappa_A) + \frac{1}{3}(1 - \kappa_A) \left[5(1 + \kappa_A) - 4\kappa_W - \frac{2}{\kappa_W} \lambda_{AW} \right] \right\} \quad (2.23) \end{aligned}$$

with $\kappa_i = m_i^2/m_{H^+}^2$ and $\lambda_{AW} = -1 + 2\kappa_A + 2\kappa_W - (\kappa_A - \kappa_W)^2$.

Substituting the fermion masses and the value of g ($G_F = g^2/(4\sqrt{2}m_W^2) = 1.16637 \times 10^{-5} \text{GeV}^{-2}$ and $m_W = 80.451 \text{GeV}/c^2$ [5]), we can calculate the fermionic and bosonic branching ratios for different values of $\tan\beta$ and Higgs boson masses.

If the mass of the charged Higgs boson is below the W boson mass, which is the case in a large fraction of the Higgs boson mass range of interest in this study, the W boson is virtual and the approximation of G_{AW} , given above for the Dalitz plot integration, is not valid. Therefore, G_{AW} has been evaluated numerically using a dedicated program [17].

If SUSY particles existed and were kinematically accessible i.e. lighter than the charged Higgs boson, the charged Higgs bosons could also decay to SUSY particles. The LEP experiments have excluded the existence of light χ^+ and χ^0 and therefore it has been assumed that light charged Higgs bosons can not decay into these particles. Decays of charged Higgs bosons into fermion pairs, or W^*A pairs, have been considered in the LEP analyses presented in publications I, II, IV and V.

2HDM Type I

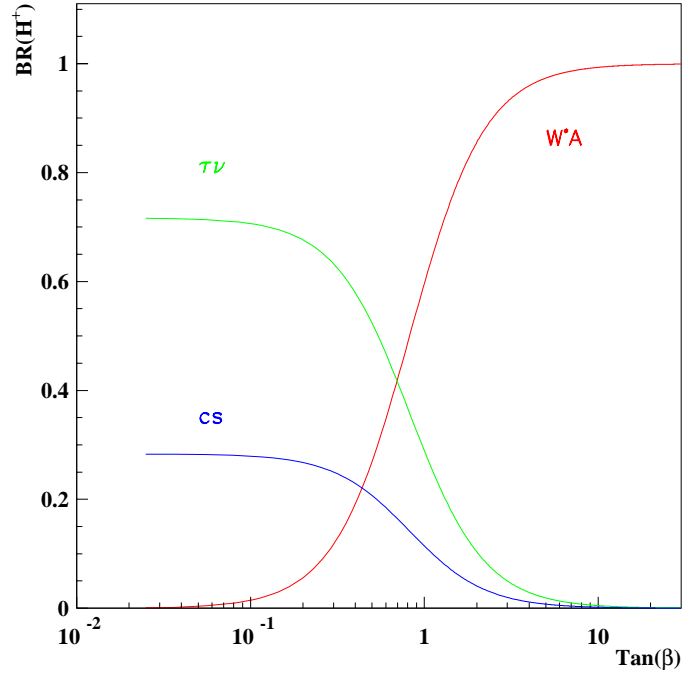


Figure 2.4: Charged Higgs boson decay branching ratios in 2HDM type I.

Chapter 3

LEP and DELPHI

The Standard Model is a sophisticated theory describing the constituents of matter and their interactions. Its development to the present level has required a large cooperative effort between theory and experiment.

This cooperation between theory and experiment continues as the high energy particle colliders provide large amounts of data for testing the theories. High precision measurements of the parameters of the Standard Model also allow more accurate extrapolations of theories beyond the Standard Model.

One of the most important experimental facilities for the precision measurements of the crucial parameters of the Standard Model and looking for evidence of alternative theories, has been the LEP collider with its four experiments at CERN.

3.1 The LEP collider

The Large Electron-Positron collider (LEP) at CERN on the Franco-Swiss border near the city of Geneva was the largest particle accelerator that has ever been built. It had a 27 km circumference storage ring situated in a tunnel about 100 m underground accelerating high energy electron and positron beams to collide with each other. The collisions happened in the four experiments, ALEPH, DELPHI, L3 and OPAL (See Fig 3.1).

LEP started operation in 1989 and enabled electrons and positrons to collide with a centre-of-mass energy that corresponds to the mass of the Z boson (at around 91 GeV). LEP operated 24 hours a day seven days a week for a period of roughly six or seven months each year (from spring to autumn).

During the first six years of running, LEP1 phase, LEP was operating around the Z mass resonance energy, 91 GeV. The yearly integrated luminosity delivered by LEP to the four experiments increased from 12 pb^{-1} in 1990 up to 65 pb^{-1} in 1994. At the end of LEP1 phase in 1996, the four LEP experiments had recorded several million Z boson decays. These large data sets were used for detailed studies of the properties of the Z boson and for performing

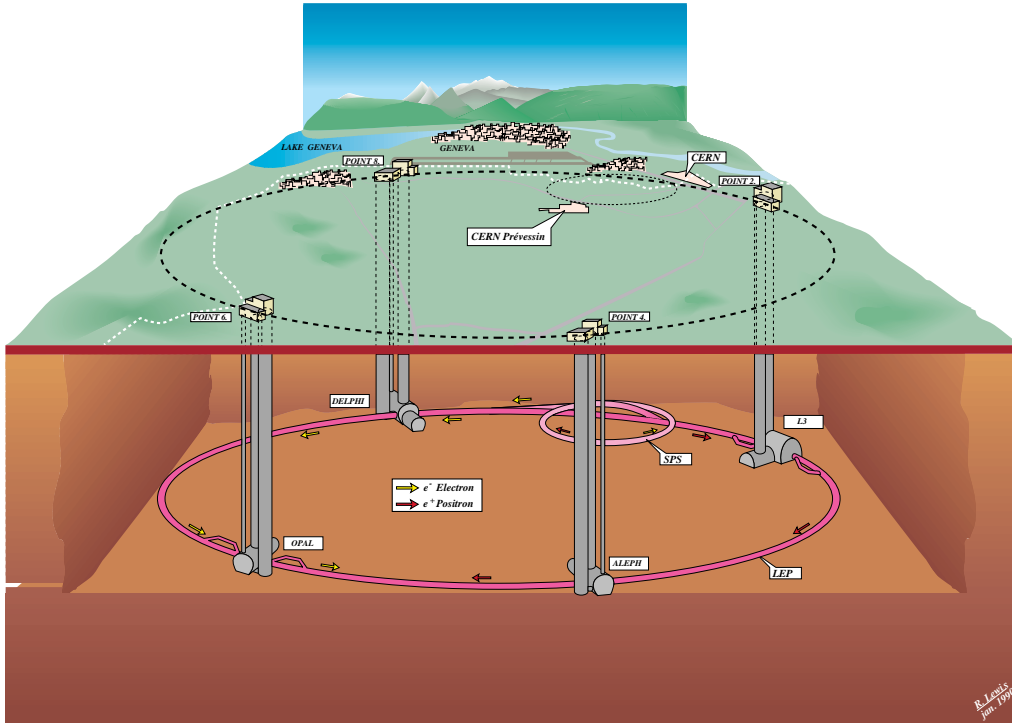


Figure 3.1: Schematic picture of the LEP collider at CERN near Geneva, Switzerland.

precision measurements of many Standard Model parameters. Evidence for new particles, such as Higgs bosons, was also searched for in Z boson decays.

In 1996, LEP started its second phase. More accelerating cavities were installed each year and the collision energy was increased reaching about 209 GeV in 2000. After the collision energy passed the W boson pair production threshold (at around 160 GeV), a large number of W boson pairs were collected in the experiments and the properties of the W boson could also be studied in detail. LEP2 phase also provided a chance to scan a large energy range in order to find the Standard Model Higgs boson or possible signals of physics beyond the Standard Model. The integrated luminosities of the high energy data samples collected by the DELPHI detector at the LEP2 phase energies are listed in Table 3.1.

3.2 The DELPHI detector at LEP

DELPHI (DEtector with Lepton, Photon and Hadron Identification) was a multi-purpose particle detector [18],[19] for LEP. It consisted of several sub-detector systems, with a barrel-shaped central part and two endcaps. With additional small angle detectors, DELPHI covered

\sqrt{s} (GeV)	luminosity (pb^{-1})
161	9.95
172	10.16
183	53.5
189	158.0
192	25.9
196	76.9
200	84.3
202	41.1
205	75.6
206.6	87.8
206.3(S6)	60.8

Table 3.1: Approximate integrated luminosities of LEP II data samples collected during the years 1996-2000. “S6” denotes data taken during a period when sector 6 of the Time Projection Chamber was not operating due to technical problems. Luminosities for 161–183 GeV are taken from publication I and luminosities for 189 GeV and above are taken from publication V.

most of the whole 4π solid angle around the interaction point, in which the LEP beams collided. A schematic view of the DELPHI detector can be seen in Fig 3.2. As for size, DELPHI was almost 10 m in length and nearly 10 m in diameter. The coordinate system used in the description of the detector is cylindrical, with the z -axis aligned along the beam axis and the $R\phi$ -plane perpendicular to the z -axis. An alternative coordinate system commonly in use to describe physics events is the polar coordinate system, with the polar angle θ defining the angle with respect to the beam axis and ϕ defining the azimuthal angle around the beam axis.

The sub-detector systems could be divided into two main categories: the tracking detectors and the calorimeters. In addition, there were some detectors that have been specifically designed for particle identification.

The tracking detectors were mainly located in the innermost part of DELPHI and they determined the momenta of the charged particles by measuring the curvature of the tracks in the 1.2 Tesla magnetic field created by a large superconducting solenoid.

Outside the tracking detectors were the calorimeters, which consisted of high density materials and measured the energies of charged and neutral particles by stopping them.

In between the tracking detectors and calorimeters were the Cherenkov detectors, which were used for identifying different charged hadrons. The outermost parts were the muon chambers that detected the muons which penetrated through all other subdetectors.

The combination of the information from all the subdetectors allowed detection and measurement of all other particle types except neutrinos, which interact with matter only very weakly.

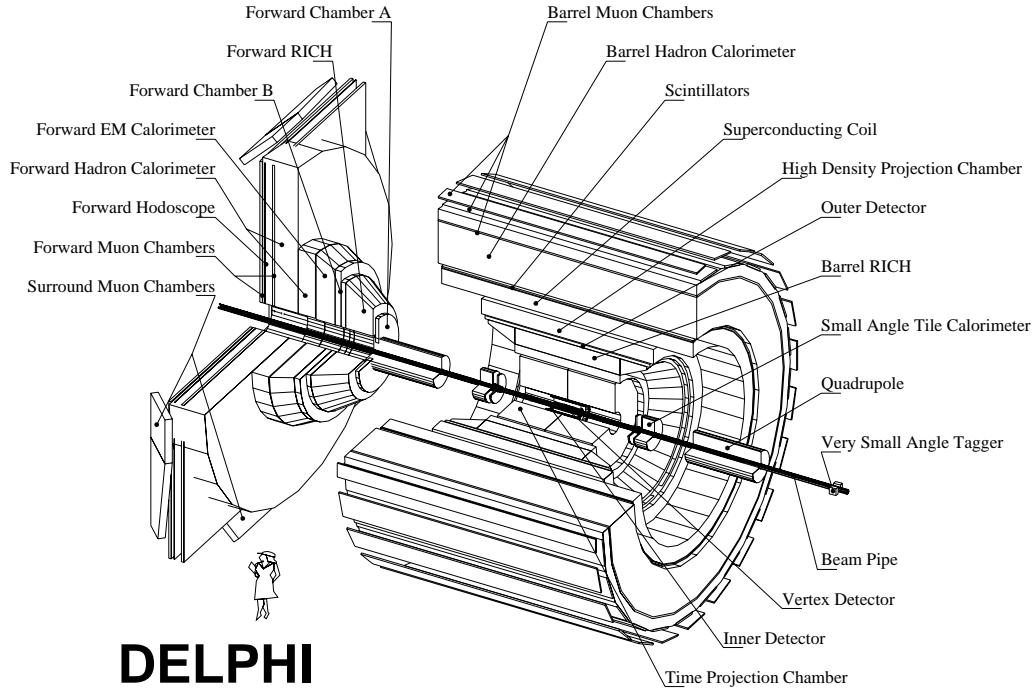


Figure 3.2: Layout of the sub-detectors of the DELPHI detector.

3.2.1 Tracking

The innermost of the tracking detectors was the Silicon Tracker. It consisted of three layers of silicon detectors at average radii of 6.3, 9.0 and 10.9 cm with each layer covering full azimuthal angle. With the excellent $7 \mu\text{m}$ $R\phi$ measurement resolution, the vertex detector allowed extrapolation of tracks into the interaction region and reconstruction and separation of primary and secondary vertices. This was essential for identification of heavy b and c quarks.

In the barrel region, the charged particle momenta were measured with high precision in the Time Projection Chamber (TPC) which was located between radii of 40 and 110 cm. The single point precision for tracks from $Z \rightarrow \mu^+\mu^-$ was $250 \mu\text{m}$ in the $R\phi$ plane and $880 \mu\text{m}$ in the Rz plane. Additional tracking information was provided by the Inner Detector (ID) at radii between 12 and 21 cm and the Outer Detector (OD), located between radii 197 and 206 cm.

Combining the tracking information of the TPC with the Vertex Detector, the ID and the OD, the precision of the DELPHI charged particle momentum measurement for tracks from $Z \rightarrow \mu^+\mu^-$ was in the barrel region ($-42^\circ \leq \theta \leq 42^\circ$) as good as

$$\sigma(p)/p = 0.6 \times 10^{-3}p, \quad (3.1)$$

where the momentum p is given in GeV/ c .

In the forward region, the limited range of the TPC was compensated for by two planar detectors: the Forward Chamber A (FCB) and Forward Chamber B (FCB) at distances of $|z| = 160$ and $|z| = 275$ cm from the interaction point. The combined momentum resolution in the forward region ($|\theta| \leq 42^\circ$) was

$$\sigma(p)/p = (1.3 - 2.7) \times 10^{-3}p, \quad (3.2)$$

where the momentum p is given in GeV/ c . In the forward region, the value changed significantly depending on which forward region detectors had coverage at the angle of the track.

3.2.2 Calorimetry

Electromagnetic calorimeters were optimised for detection and energy measurement of electrons and photons. The barrel calorimeter, High Density Projection Chamber (HPC), was located at radii from 208 cm to 260 cm. It contained lead converters with a total radiation length of $18 \times \sin \theta$.

The relative precision of the HPC energy measurement was

$$\sigma(E)/E = 0.043 + 0.32/\sqrt{E}, \quad (3.3)$$

where the energy is given in GeV. The angular precisions of high energy photons were 1.7 mrad in ϕ and 1.0 mrad in θ .

In the forward region, electromagnetic energy was measured using the Forward Electromagnetic Calorimeter (FEMC), which consists of Cherenkov lead glass blocks with a depth of 40 cm corresponding to 20 radiation lengths. The Cherenkov signal was read out by using photomultipliers.

The relative precision of the FEMC energy measurement was

$$\sigma(E)/E = 0.03 + (0.12/\sqrt{E}) + (0.11/E), \quad (3.4)$$

where the energy is given in GeV.

The barrel Hadron Calorimeter (HCAL) consisted of 20 layers of streamer tubes sandwiched between 5 cm layers of iron and it was located outside the magnet solenoid. The endcap HCAL had a sampling depth of 19 layers. The HCAL was used for the energy measurement of charged and neutral hadrons and it also acted as the return yoke of the magnet.

The energy resolution of the hadron calorimeter was

$$\sigma(E)/E = 0.21 + 1.12/\sqrt{E} \quad (3.5)$$

where the energy is given in GeV.

3.2.3 Particle identification

Different particle types, photons, electrons, muons, charged hadrons and neutral hadrons, can usually be distinguished from each other in large detector systems due to their very different interaction mechanisms in different tracking detectors and calorimeters. In addition, with the DELPHI detector, it was possible to distinguish charged hadrons with different masses from each other. A commonly used method is the specific energy loss measurement in the main tracking detector TPC. Another method, specific to DELPHI, was to use specific particle identification detectors, Ring Imaging Cherenkov (RICH) detectors.

The specific ionisation energy loss, dE/dx , depends on the mass and momentum of a charged hadron. The sense wires of the DELPHI TPC provided 192 ionisation measurements per track, allowing separation between protons, pions and kaons.

RICH detectors measure the emission angle of Cherenkov radiation emitted by charged particles traversing a medium with a speed faster than the speed of light in this specific medium. The Cherenkov angle depends on the velocity of the particle and, combining the velocity measurement with the momentum to mass ratio information measured in tracking detectors, it is possible to extract the particle masses and therefore to separate charged hadron types from each other.

DELPHI RICH contained two radiators, a liquid radiator, optimised for particle identification in the momentum range from 0.7 to 8 GeV/ c , and a gas radiator, for the momentum range from 2.5 to 25 GeV/ c . Cherenkov photons created in both radiators were collected using planar photodetectors which imaged a ring of photons with a radius depending on the Cherenkov emission angle.

Information from all particle identification detectors was combined using particle identification algorithms providing proton, kaon and pion tags to be used in various analyses.

3.2.4 Event reconstruction

Combination of the tracking and calorimetry information allows the reconstruction of event energy flow i.e. the full reconstruction of energies of charged and neutral particles.

Fig 3.3 shows an event display of a multihadron event recorded by DELPHI at the highest centre-of-mass energy of LEP, 208.8 GeV. The event is projected in the $R\phi$ plane and two subdetectors are shown in the event display: the six segment main tracker, the Time Projection Chamber, and the 24 segment electromagnetic calorimeter, the High Density Projection Chamber. The fitted trajectories of charged and neutral particles are shown in the figure. In addition, a jet clustering algorithm has been used and the momentum vectors of the four reconstructed jets are shown as black arrows. The hadronisation process and jet clustering are discussed in detail in the following chapter.

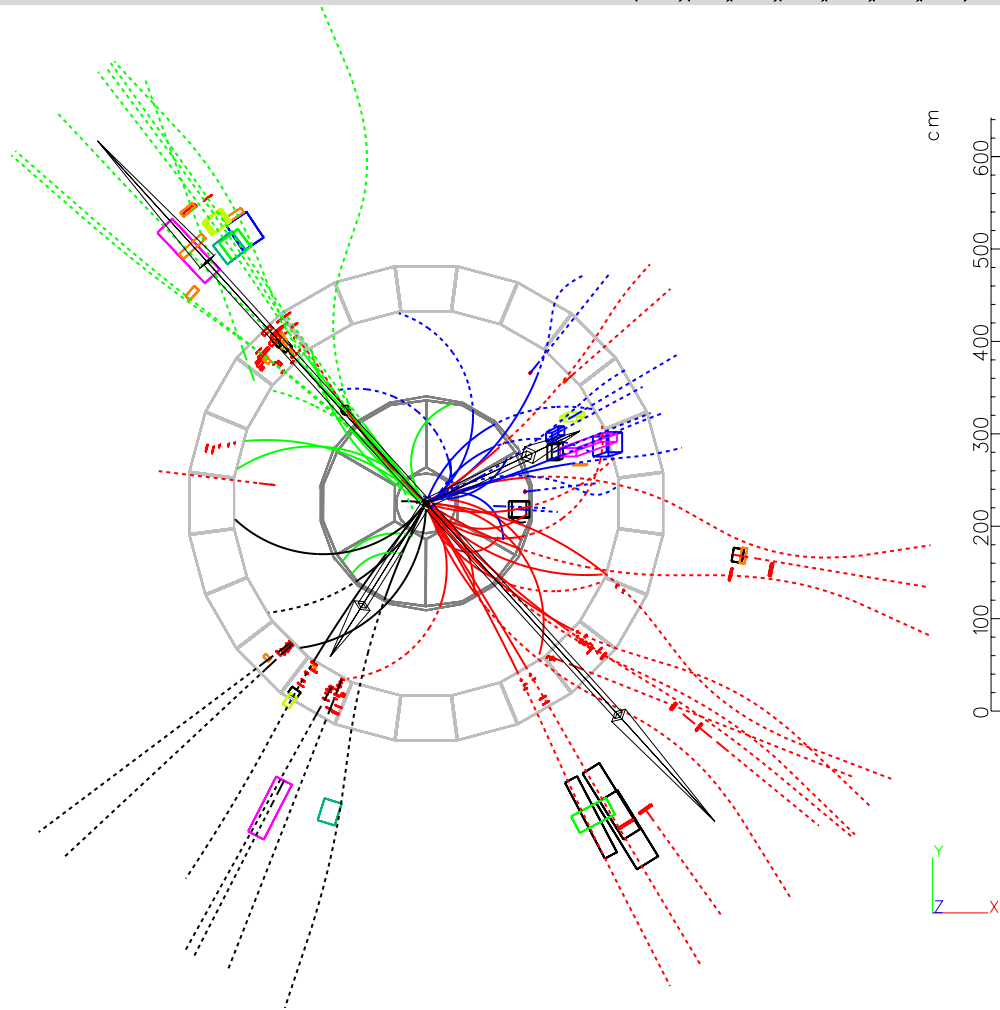


Figure 3.3: A four-jet event recorded by the DELPHI detector at 208.8 GeV centre-of-mass energy. Two detectors are shown: the six segment main tracker (TPC) and the 24 segment electromagnetic calorimeter (HPC). The solid curved lines are charged tracks reconstructed in tracking detectors. The dashed lines are either extrapolations of the reconstructed charged tracks or fitted neutral particle trajectories based on measured energy deposits in calorimeters. The rectangular objects, roughly 100-200cm outside the HPC, are energy deposits measured in the hadronic calorimeter (HCAL). The black arrows show the momentum vectors of the four reconstructed jets. This event is most compatible with the hypothesis of being a background event where a pair of W bosons decays into four quarks.

Chapter 4

Reconstruction methods for hadronic final states

If charged Higgs bosons are produced in collider experiments, their final decay products can be detected and measured in particle detectors. Information about the properties of the Higgs bosons themselves can be obtained by reconstructing the decay processes, step-by-step, backwards in time.

4.1 Monte Carlo simulations

Event reconstruction methods for hadronic decays of heavy bosons are developed and tested by using large sets of Monte Carlo simulated decay processes. With simulated data, the properties of a reconstructed heavy boson can be compared to the known properties of the initial simulated bosons, and the efficiencies and resolutions of the experimental reconstruction methods can be estimated. This method requires detailed understanding of all physics processes involved in the decay chains and particle detectors. Any difference between the simulations and real physics processes would lead to a bias or a systematic error in the efficiency and resolutions functions.

2HDM models give predictions for the decay processes of charged Higgs bosons. Further decays and interactions of the Standard Model particles produced in Higgs boson decays are described by the Standard Model. In particular, the electroweak processes, such as decays of leptons, can be calculated with high precision. In the case of strong interaction processes, the Standard Model is not able to give quantitative descriptions or predictions for low energy processes and parametrised hadronisation models have to be used.

The reliability of the simulations of the production and decay processes, hadronisation models and detector responses in the LEP experiments were tested using the large amounts of Z boson decays recorded at LEP1. By performing detailed comparisons between real data and simulations for many known Standard Model processes, a high level of confidence was obtained for the reliability of results.

4.2 Hadronisation

The strong interaction has a peculiar property. In contrast to other interactions, the strength of the attractive force between quarks increases as a function of the distance between quarks. As a consequence, quarks are bound together by the strong interaction and can not be detected as free particles, but are indirectly observed as constituents of colourless bound states, hadrons. This phenomenon is called confinement [2].

In a hadronic decay of a heavy boson, such as a Higgs, Z or W boson, the mass of the boson is transformed into the kinetic energy of the quark and anti-quark, which fly in opposite directions with momenta corresponding to half of the boson mass. At such a high momentum transfer, the strong coupling constant α_s has a low value allowing the use of perturbative QCD for calculations. The perturbative parton cascade can be used to describe the emission of gluons and the creation of $q\bar{q}$ pairs down to momentum transfers of the order of few hundred MeV [20],[21].

At low momentum transfer values, the coupling strength α_s becomes larger and the perturbation theory can not be used for calculation. Presently there is no theory that allows calculations of low energy QCD processes involved in hadron formation processes. To describe the formation of hadrons, we can only use probabilistic hadronisation models which rely on experimental measurements of relative fractions of different species of final state hadrons in different processes [22].

In most of the LEP1 and LEP2 analyses involving QCD processes, hadronisation was simulated according to the Lund string model [23]. In a string model, hadronisation happens in a massless relativistic colour field “tube”, which spans between the two initial quarks. Additional energetic gluons can be emitted resulting in kinks in the string. The string breaks into $q\bar{q}$ pairs which are finally combined into hadrons. As the final state hadrons are created inside the string, they can not be, strictly speaking, taken to be coming from one initial quark. However, the large kinetic energy of the initial quark gives a significant boost to hadrons produced at the ends of the strings near the initial quark. These most energetic hadronisation products form a narrow jet of particles carrying most of the initial quark’s momentum. An additional jet can be formed if an energetic gluon with a large angle to the quarks has been emitted in the early stage of the parton cascade process.

In all analyses described in this thesis, the parton cascade and hadronisation processes from initial $q\bar{q}$ pair down to final state hadrons were simulated with the PYTHIA software [24] which uses the Lund string scheme. The numerous parameters of the PYTHIA hadronisation description had been tuned by using data from millions of Z boson decays recorded at LEP1. The Higgs or W bosons in the signal and background events in the DELPHI searches for charged Higgs bosons had masses close to the Z boson mass, which guaranteed that the tuning done at Z boson energy was also valid for these processes.

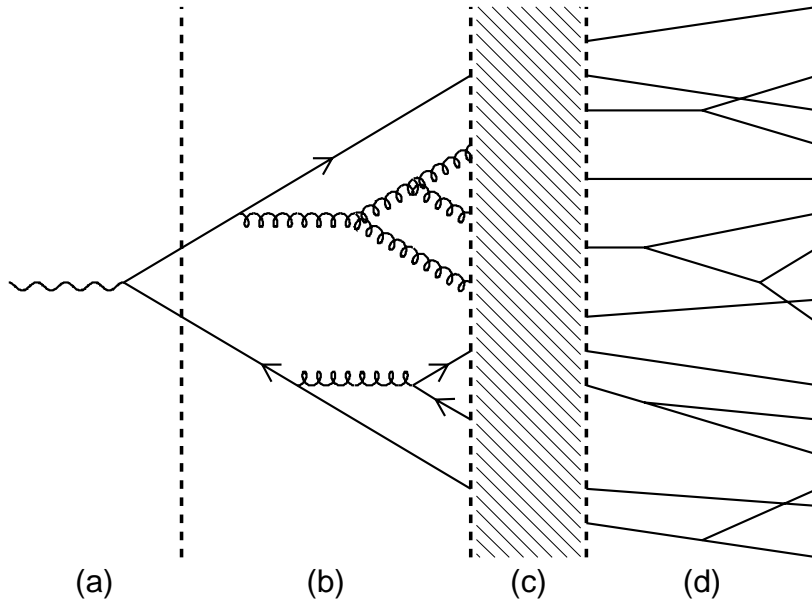


Figure 4.1: A schematic representation of the hadronisation process in a decay of a boson to a quark pair. (a) electroweak production of primary $q\bar{q}$ pair, (b) perturbative parton cascade, (c) hadronisation and (d) decay of unstable hadrons.

4.3 Jet reconstruction and flavour tagging

The initial decay products of the Higgs bosons, the initial quark-antiquark pair, can not be detected directly, but their properties can be reconstructed with reasonable accuracy using the final state particles that are measured in the detectors.

Jet clustering algorithms are used to combine the particles that are most likely to originate from the same initial quark. If this assignment is successful, the summed four-momentum of the particles in each jet gives a good estimate of the four-momentum of the initial quark. As already mentioned, this is a simplified picture of the hadronisation process, but in most cases the jets give a good approximation for the directions and energies of the initial quarks. All publications, I–VII, included in this thesis depend on jet clustering algorithms as a tool for measuring the four-momenta of objects in hadronic decay processes.

Many algorithms with different basic principles are available. The most common ones use an approach in which all particles are initially regarded as separate clusters. Algorithms start by initially combining the two closest clusters into one cluster and then recalculating the distances between all clusters. Then, the closest clusters are again combined and this procedure is repeated until all clusters are separated by at least a certain predefined minimum value of the distance parameter. Different algorithms use different definitions of the parameter (e.g. y_{cut} or d_{join}) for the distance between two clusters. The simplest algorithms directly use the angle between the clusters and more sophisticated algorithms use the invariant mass of

the cluster pair (or some similar quantity) as a measure. The algorithm used in most of the analyses described here is the DURHAM jet clustering algorithm [25], which uses the following definition for the distance Y_{ij} between two clusters i and j

$$y_{ij} = \frac{2(1 - \cos \theta_{ij}) \min\{E_i^2, E_j^2\}}{E_{vis}^2}, \quad (4.1)$$

where θ_{ij} is the angle between the two clusters, E_i are the cluster energies and E_{vis} is the visible energy in the events i.e. the sum of the energies of all measured clusters. This algorithm joins together the two clusters that have the smallest transverse momentum between them.

If the cut value of the clustering distance is fixed before clustering, the number of resulting jets can vary from event to event. Another approach is to predefine the required number of jets and stop clustering when exactly wanted number of jet is obtained. The latter method is called “forcing event to n jets”. Both methods were used in the analyses described in publications I–VII.

The flavour of the initial parton, from which the jets originate, can be also identified. In particular, the heavy b quarks can be identified with a high efficiency and purity using the high precision tracking resolution of the silicon vertex detector. The heavy B mesons, containing a b quark, have a long enough life time allowing them to fly a distance of few millimetres before decaying. By extrapolating the particle tracks from the silicon vertex detector backwards into the interaction point, it is possible to measure the so-called impact parameter, which is the smallest distance of approach between the interaction point and the extrapolated track. For particles originating from the primary vertex, the impact parameter is zero within the precision of the extrapolation. The decay products of heavy mesons, which do not originate from the primary interaction point but from the decay location of the meson, have larger impact parameter values. If there are more than one large impact parameter tracks in the event, a secondary vertex can be searched for and if the large impact parameter tracks have small impact parameters with respect to that vertex point, the decay location of the heavy meson can be determined. Fig. 4.2 shows an example of an event with many large impact parameter tracks that form two secondary vertexes, 1 – 2 cm away from the interaction point. These secondary vertexes are, with very high probability, decay locations of B mesons. Effective b quark jet tagging is a necessary requirement for successful jet pairing in the analyses described in publications VI and VII.

Identification of other quark flavours is more difficult, but c and s quarks can also be separated from the light u and d quarks with a more moderate separation power. Special jet flavour tagging algorithms have been developed for this use. Discussion about c and s quark identification methods can be found in publications I, II, IV and V.

4.4 Mass reconstruction and kinematic fits

Due to energy and momentum conservation, the masses of the Higgs boson candidates can be calculated from the measured four-momenta of the jets. The jet direction and energy mea-

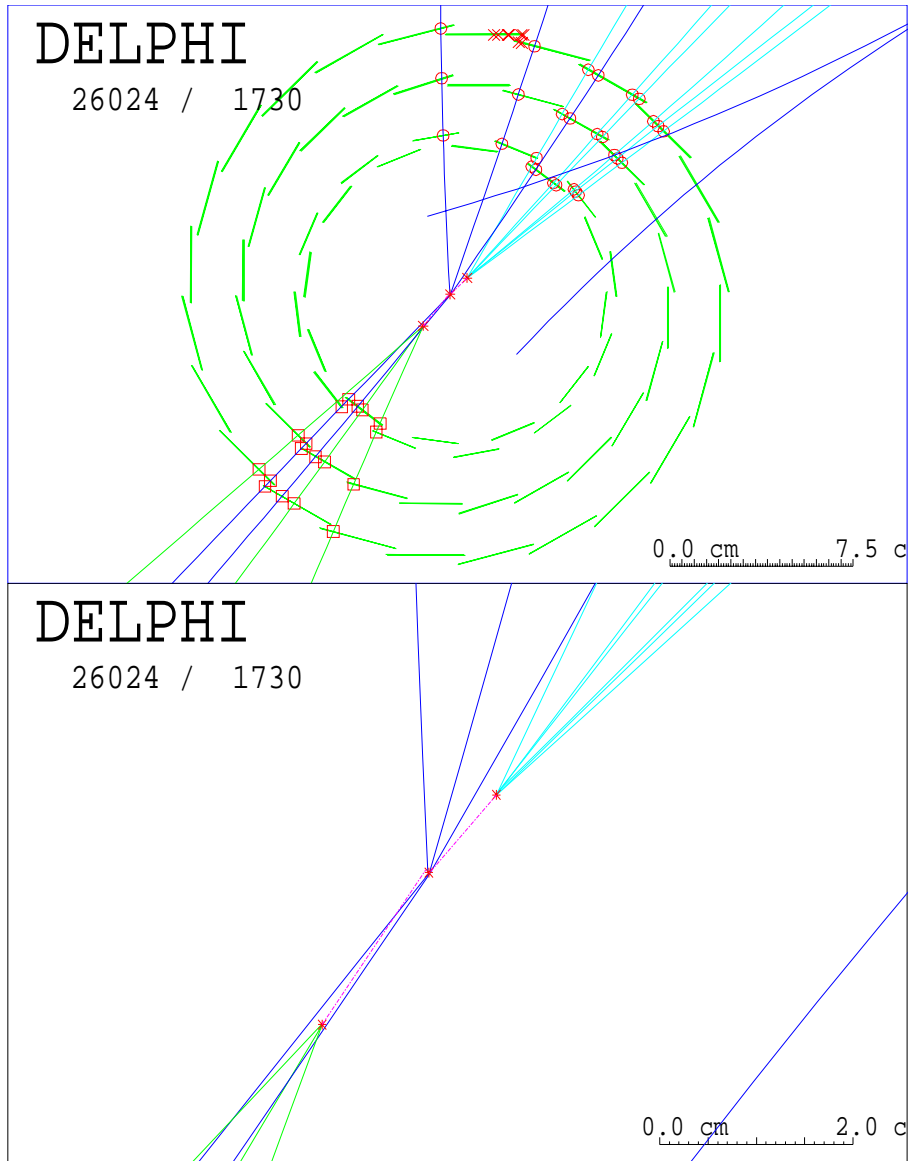


Figure 4.2: An xy-plane projection view of an event in the silicon vertex detector. The upper figure shows the three detector layers, the detected hits and the fitted tracks of detected charged particles. The lower figure shows magnification of the interaction region. The primary vertex in the centre and two secondary vertices 1-2cm away from the primary vertex are clearly visible. The two reconstructed secondary vertices originate from decays of heavy mesons containing b quarks.

measurements always have some uncertainty and that leads to uncertainties in the reconstructed masses of the Higgs bosons.

The mass resolution of a Higgs boson candidate can be improved by using kinematic fits. Fits modify the jet energies and momentum vectors with predefined boundary conditions, which are based on energy and momentum conservation and known properties of particles. A four-constraint fit (4-C fit) requires the total energy, and the three components of the total momentum of the four-jet system after fitting, to be equal to the total energy and momenta of the initial colliding electron-positron system. A five-constraint (5-C) fit uses, as an additional constraint, the information that the masses of the two Higgs bosons are equal.

The kinematic fits used in publications I-VII were performed using the PUFITC program [26, 27, 28]. The inputs for this program are the measured four-momentum vectors and the resolutions of the momentum and angle measurements of the DELPHI detector.

The fitted jet momentum vector, \vec{p}_j^f , is [28]

$$\vec{p}_j^f = \exp(a_j)\vec{p}_j^m + b_j\vec{p}_j^b + c_j\vec{p}_j^c, \quad (4.2)$$

where \vec{p}_j^m is the measured momentum vector, a_j , b_j and c_j are fitted parameters and \vec{p}_j^a and \vec{p}_j^b are vectors with 1 GeV/c length perpendicular to the measured jet momentum vector. Parameter $\exp(a_j)$, therefore, determines the scaling factor for the jet momentum, and parameters b_j and c_j the change in the jet direction. The energy of the jet, E_j^m and therefore also the mass of the jet, is scaled with the same factor $\exp(a_j)$ as the momentum.

Parameters of the fit are found by requiring the fit constraints to be filled with a minimal value of the χ^2 of the fit:

$$\chi^2 = \sum_j \frac{(a_j - a_0)^2}{\sigma_{a_j}^2} + \frac{b_j^2}{\sigma_{b_j}^2} + \frac{c_j^2}{\sigma_{c_j}^2}, \quad (4.3)$$

where a_0 is the expectation value of a_j and σ_{a_j} , σ_{b_j} , σ_{c_j} are the resolutions of the momentum and direction measurements of the DELPHI detector.

A small value of the χ^2 of the fit indicates that only a little modification of the jet momenta was needed to fulfil the event configuration hypothesis. The opposite case, a large value of the χ^2 , indicates that either something went wrong in the initial jet reconstruction or the event is a background event with a different kind of jet topology. 4-C and 5-C fits were used to improve the mass resolution and to find the correct jet pairings in four-jet final states in publications I-V.

In publications VI and VII, we applied the kinematic fit procedures for much more complicated final states, possibly produced at future high energy linear colliders. Up to nine constraints were used for kinematics of an eight jet final state in $e^+e^- \rightarrow H^+H^- \rightarrow t\bar{t}b\bar{b} \rightarrow W^+b\bar{b}W^-b\bar{b} \rightarrow 8 \text{ jets}$ process. The first four constraints were the usual energy and momentum conservations. Four additional constraints came from the known masses of W bosons and t quarks. The last constraint was the condition that the Higgs bosons have equal masses. The same procedure

was also shown to work for the alternative $H^+H^- \rightarrow W^+h^0W^-h^0$ decay process, where the t quark mass constraints were replaced by ones using the mass of the h^0 boson. This decay process would be possible only if the h^0 mass were significantly lower than the charged Higgs boson mass. In this case, the mass of h^0 would already be measured with high precision at the time when the heavier charged Higgs bosons could be searched for.

4.5 Finding the correct quark-antiquark pairs

In the case of two heavy bosons decaying into four quarks, which then result in four jets, there are three possible ways to combine jets into two pairs.

In general, it is not possible to distinguish between quarks and antiquarks. The performance of the jet flavour tagging is also not sufficient to be able to identify the c and s quark jets with such high efficiency that this information could be used for reducing the combinatorics of pairing.

The most powerful tool for pairing is to use the kinematic properties of the event, namely the fact that the two charged Higgs bosons should have equal masses. This can be done either by finding after the 4-C fit, the jet pairing which minimises the difference between the two boson masses, or by performing the 5-C fit for all three pairings and then choosing the pairing which minimises the χ^2 of the fit. The 5-C method was found to be slightly more efficient in finding the correct pairing with about 80% efficiency. This method was used in the searches for charged Higgs bosons described in publications I, II, IV and V.

A new method for rejecting significant fraction of the wrong jet pairings was developed. It uses the fact that the hadrons in the jets do not originate from free quarks but from the colour field span between the quark and the antiquark.

Looking at this process in the rest frame of the quark-antiquark pair, these two initial partons are flying in opposite directions i.e. they are back-to-back. In this picture, the hadrons are produced in the colour field flux tube or string, which spans between the initial quarks. In the absence of hard gluon emission, which has a reasonably low probability, there is only little transverse momentum in this system and all particles should therefore be quite well-aligned along the quark-antiquark axis.

In the case of a four-jet event, there are three pairing hypotheses with two di-jet pairs in each hypothesis. These three hypotheses were tested one-by-one for each event. Firstly, all particles were boosted into the rest frame of the two di-jet pairs and the particles' transverse momenta p_t with respect to the di-jet axis were calculate .These particles were then assigned to the di-jet in which they have minimum transverse momenta and finally all transverse momenta were summed up. These transverse momenta sums of each three pairing hypotheses were compared to each other and the one with lowest sum was chosen to be the preferred pairing.

The efficiency of this method was significantly lower than the efficiency of the 5-C fit χ^2 minimisation. Therefore, 5-C fit χ^2 minimisation was used for choosing the pairing for mass reconstruction, but if the p_t sum method chose different pairing, the event was labelled as being potentially wrongly paired. This label, called p_t -veto, was used for suppression of background

resulting from wrongly paired W boson pairs in the analysis optimised for Higgs boson masses below the W mass, as described in publication IV. At higher centre-of-mass energies and higher collected integrated luminosities, which were available for analyses described in publication V, the main region of interest was at the W mass peak, where this method was no longer as efficient as at a lower mass range.

In the eight-jet final state analyses described in publications VI and VII, the combinatorics of jet pairings and assignments were much more complicated. Fortunately, much more useful information was also available. Four of the jets could be b -tagged and separated from the four light quark jets. The known t quark, W boson and h^0 boson masses could also be used to find di-jet systems with masses compatible with the hypothesis of being t , W or h^0 . At the end, the number of possible combinations was limited to two, and the final decision was made choosing the one which minimised the χ^2 of the fit. Different decay process hypotheses could be fitted for each event and by comparing the χ^2 values of the hypotheses, it was possible to separate different signal hypotheses from each other, and to reject background events.

Chapter 5

Interpretation of the DELPHI H^+H^- search results

Each of the analyses of different decay channels provides information about the observed number of Higgs boson pair candidate events and, for each event, the values of several variables describing the properties of the Higgs boson candidates. This information has to be interpreted statistically i.e. it needs to be converted into the form of probabilities and confidence levels for the existence or non-existence of the Higgs bosons in the data.

5.1 The likelihood ratio method for confidence limits

The test statistic used in this method is a likelihood ratio, $Q(\vec{X})$, which is the ratio of the probability densities of two alternative hypotheses [29]. The two hypotheses in the case of new particle searches are the “signal+background” hypothesis and the “background only” hypothesis, and the likelihood ratio in this case is

$$Q = \frac{\mathcal{L}(\vec{X}, s + b)}{\mathcal{L}(\vec{X}, b)} \quad (5.1)$$

where $\mathcal{L}(\vec{X}, h)$ is the probability (or likelihood) of observing the given experimental result \vec{X} within hypothesis h .

In traditional counting experiments, the probability would simply be defined as the Poisson probability to observe n_{obs} signal event candidates in the experiment.

In sophisticated experiments, there is much more information available. For each signal candidate event, the values of many variables are compared to the simulated probability distributions of the signal+background hypothesis and the background only hypothesis. Each individual event can therefore be assigned a signal to background likelihood value.

The number of signal event candidates and detailed information of each candidate from all analyses of different decay channels and centre-of-mass energies is finally combined into one single likelihood ratio Q [29]

$$Q = \frac{\prod_{i=1}^{N_{chan}} \frac{e^{-(s_i+b_i)}(s_i+b_i)^{n_i}}{n_i!} \prod_{j=1}^{n_i} \frac{s_i S_i(x_{ij}) + b_i B_i(x_{ij})}{s_i + b_i}}{\prod_{i=1}^{N_{chan}} \frac{e^{-b_i} b_i^{n_i}}{n_i!} \prod_{j=1}^{n_i} B_i(x_{ij})} \quad (5.2)$$

which can be simplified to [29]

$$Q = e^{-s_{tot}} \prod_{i=1}^{N_{chan}} \prod_{j=1}^{n_i} \left(1 + \frac{s_i S_i(x_{ij})}{b_i B_i(x_{ij})} \right), \quad (5.3)$$

where n_i is the number of observed candidates in each channel, x_{ij} is the value of the discriminating variable for each of the candidates, s_i and b_i are the integrated signal and background rates for each channel, s_{tot} is the total signal rate for all channels, and $S_i(x)$ and $B_i(x)$ are the probability distribution functions of the discriminating variable for the signal and background of channel i .

Monte Carlo simulations are used to generate a large number of artificial ‘‘Gedanken experiments’’, simulating the measurement of the final likelihood ratio Q with and without signal. The Q_{obs} value of real data collected by the experiment is then, at the end, compared to the distribution of the Q values in the Gedanken experiments.

Final confidence levels are then derived from the Q value distribution[29]. The confidence level of the signal+background hypothesis, CL_{s+b} is,

$$CL_{s+b} = P_{s+b}(Q \leq Q_{obs}) \quad (5.4)$$

and the confidence level of the background only hypothesis, CL_b , is

$$CL_b = P_b(Q \leq Q_{obs}) \quad (5.5)$$

where $P(Q \leq Q_{obs})$ are the integrals of the simulated Q probability distributions (from $-\infty$ to Q_{obs}).

The confidence level for the existence of signal, CL_s , is finally defined as

$$CL_s \equiv \frac{CL_{s+b}}{CL_b} \quad (5.6)$$

and the signal hypothesis can be excluded at the confidence level CL when

$$1 - CL_s \leq CL. \quad (5.7)$$

5.2 Mass and cross-section limits

The likelihood ratio method was used to calculate the signal observation and exclusion confidence levels for signal hypotheses in different models. A signal-like excess of events, with a significance of five standard deviations, was required for a discovery of a new particle. If no discoveries were obtained, exclusion limits could be set for models which would have predicted results that were inconsistent with the actual observation.

The results of the DELPHI searches for charged Higgs bosons are presented in publications II, IV and V. No significant deviations from the Standard Model predictions were observed and the conclusion was that no evidence for the existence of Higgs bosons was found. Monte Carlo simulated samples of charged Higgs bosons were used to evaluate the sensitivity of the DELPHI searches for different 2HDM signal hypotheses and, based on these simulations, the existence of a low mass charged Higgs boson could be excluded.

These results were visualised using exclusion limit plots. For 2HDM type II, there are two free parameters: the mass of the charged Higgs boson and the leptonic branching ratio. The exclusion limit plot, see Fig. 5.1 (from publication number V), shows the 95% confidence level excluded area in the mass versus branching ratio plane for 2HDM type II. A 95% confidence level lower mass limit for the charged Higgs boson, independent of the leptonic branching ratio, was set at $74.4 \text{ GeV}/c^2$ for 2HDM type II.

In 2HDM type I, there are more free parameters: the mass of the charged Higgs boson, the value of $\tan \beta$ and the mass of the A^0 Higgs boson. The results were visualised in the same way as in the model type II case, as exclusion plots in a two dimensional plane, as can be seen in Fig. 5.2 (from publication V). In this case, the plane is $\tan \beta$ versus the mass of the charged Higgs boson, and the mass of A^0 boson is fixed for each plot. A 95% confidence level lower mass limit for the charged Higgs boson, independent of the leptonic branching ratio, can be set at $76.7 \text{ GeV}/c^2$ for 2HDM type I.

The mass limits and exclusion plots above assume that the production rate of charged Higgs bosons follows the 2HDM formulas presented in section 2.6. The DELPHI search results were also presented in a more model independent form, setting upper limits for the pair-production cross-section of charged Higgs bosons. Fig. 5.3 (from publication V) shows the 95% upper limits for the pair-production cross-section for the three possible fermionic decay channels. Similar cross-section limit plots for bosonic decay hypotheses are also available in publication V. 95% confidence level lower mass limits can be extracted from these plots for any model which predicts production cross-sections different from the 2HDM prediction.

DELPHI

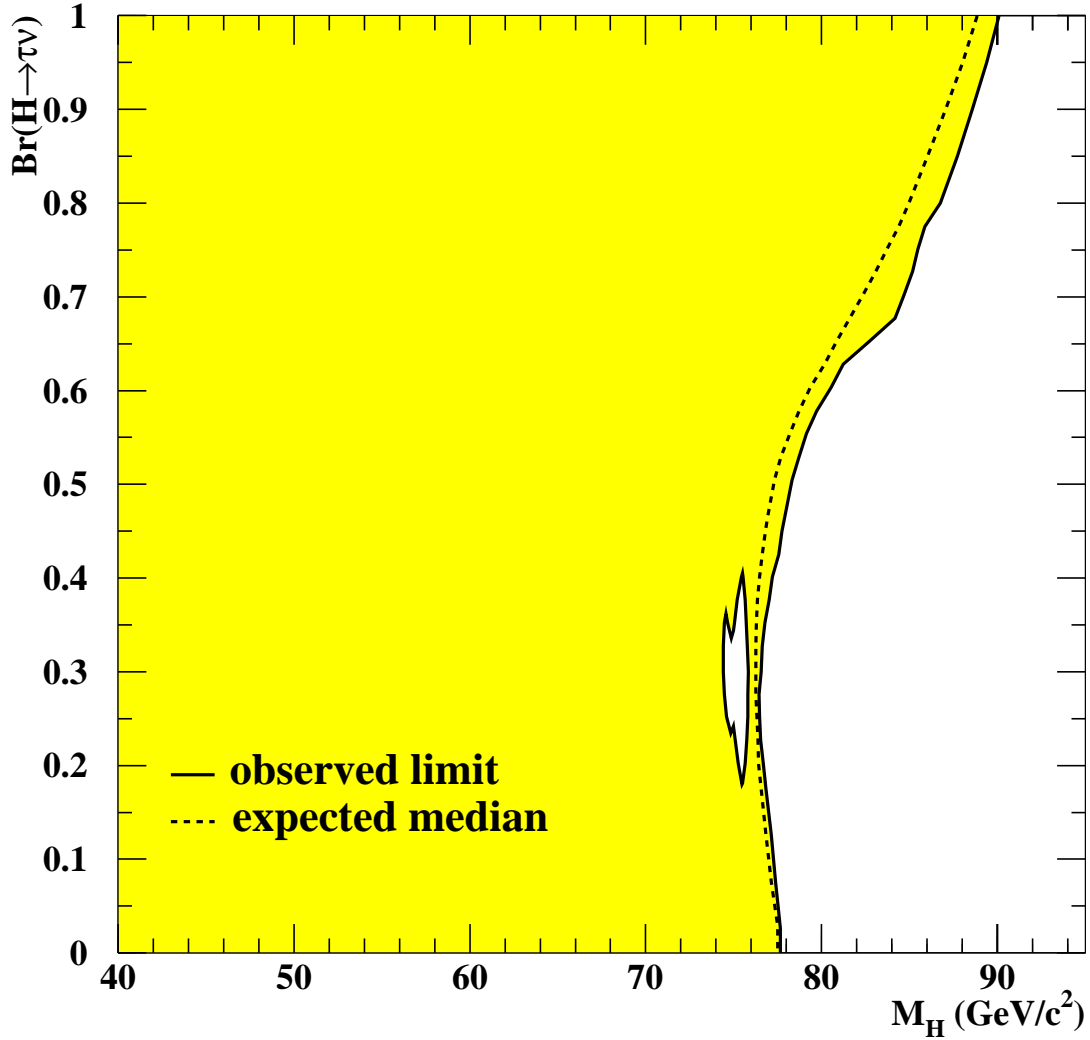


Figure 5.1: The observed and expected exclusion regions at 95% confidence level in the plane of $BR(H \rightarrow \tau^- \bar{\nu}_\tau)$ vs. M_{H^\pm} . These limits were obtained from a combination of the search results in the $\tau^- \bar{\nu}_\tau \tau^+ \nu_\tau$, $c \bar{s} \tau \nu$ and $c \bar{s} \bar{c} s$ channels at $\sqrt{s} = 189\text{--}209$ GeV, under the assumption that the $W^* A$ decay is forbidden.

DELPHI

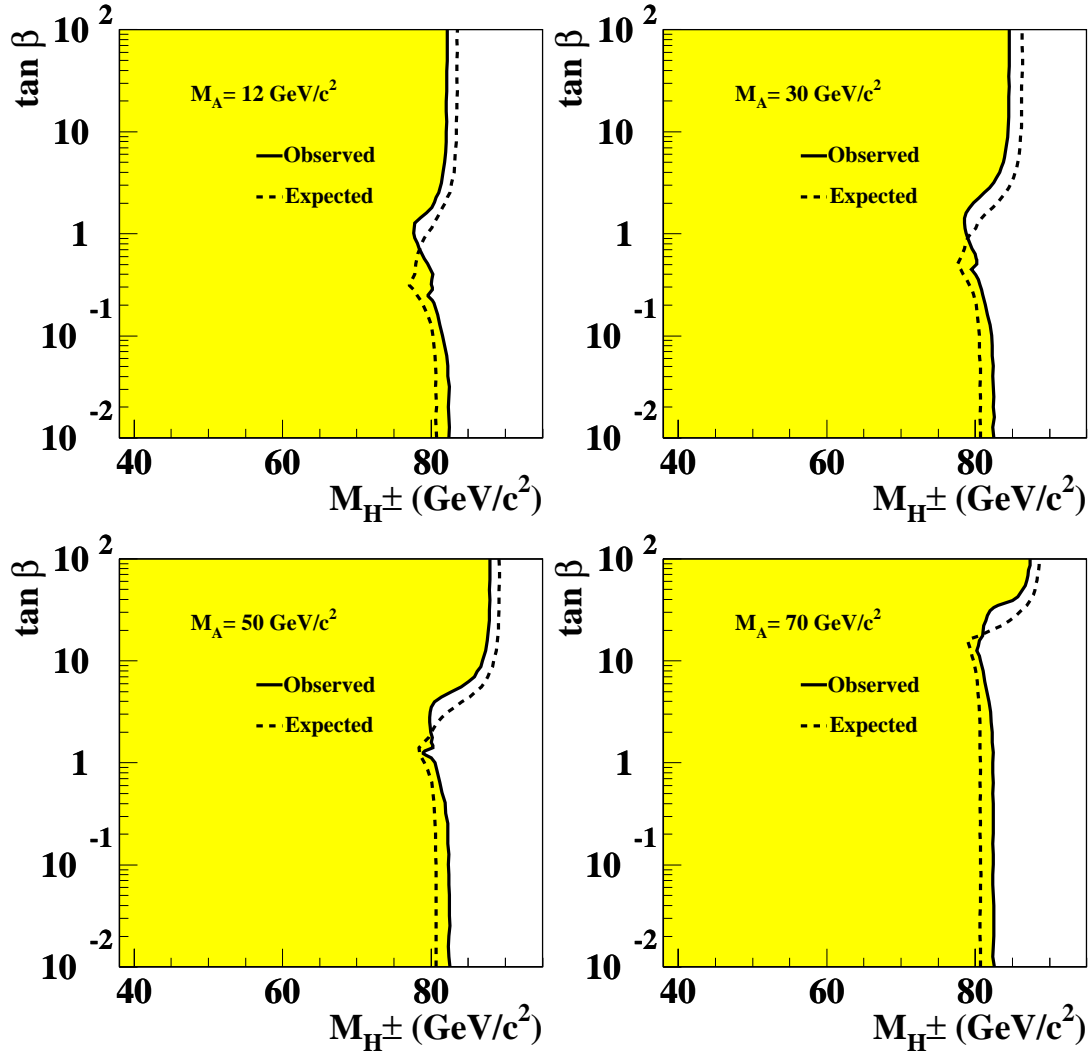


Figure 5.2: The observed and expected exclusion regions at 95% confidence level in the plane of $\tan\beta$ vs. M_{H^\pm} in the framework of type I Two Higgs Doublet Models. These limits were obtained from a combination of the search results in all studied channels, with or without W^*A decays, at $\sqrt{s} = 189\text{--}209 \text{ GeV}$, for different A masses.

DELPHI

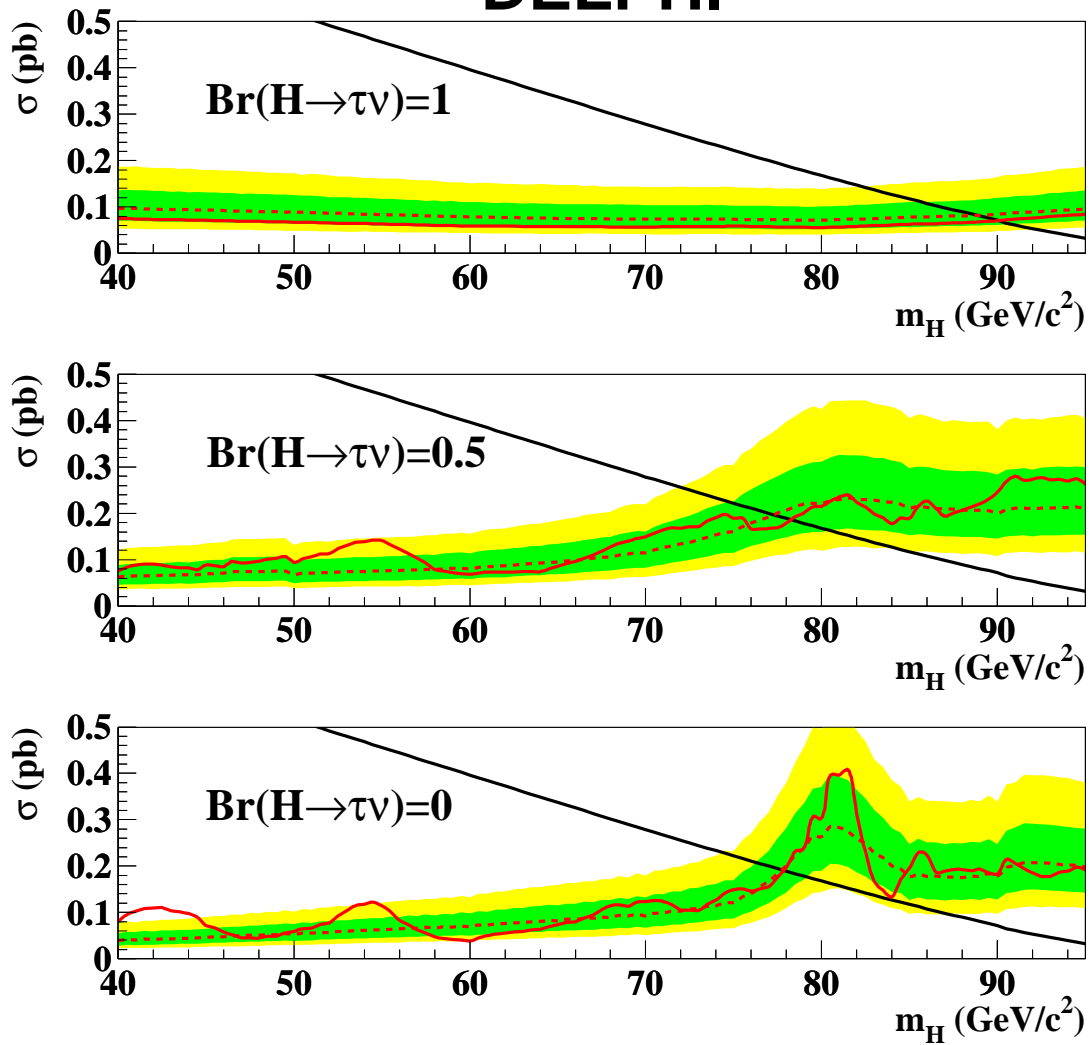


Figure 5.3: Upper limits for the cross-section of pair production of charged Higgs bosons at 95% confidence level, for different $\text{BR}(H \rightarrow \tau^- \bar{\nu}_\tau)$, under the assumption that the W^*A decay is forbidden. The dashed curve shows the expected upper limit with one and two standard deviation bands and the solid curve is the observed upper limit of the cross-section for the background only hypothesis. The solid black diagonal curve shows the two Higgs doublet model prediction. Cross-sections are given for 206.6 GeV centre-of-mass energy.

Chapter 6

H^+H^- search results of other experiments

Searches for charged Higgs bosons have been performed by many experiments operating at different kinds of colliders. All four LEP experiments have looked for pair production of charged Higgs bosons. Indirect evidence for their existence has been also looked for in lower energy e^+e^- collider experiments. Searches have also been performed at hadron colliders.

6.1 Other LEP experiments and the LEP combination

The other LEP experiments, ALEPH, L3 and OPAL have performed similar searches for charged Higgs bosons. They have looked for Higgs boson decays into $cscs$, $cst\nu$ and $\tau\nu\tau\nu$ and the results [30], [31], [32], [33] are similar to the DELPHI results.

By summer 2001, all four LEP experiments produced preliminary results of the searches for charged Higgs bosons using all high energy data collected at LEP2. A preliminary combination of these results was done within the LEP working group for Higgs boson searches and the results of this combination were also presented at conferences [34].

As the performances of the experiments were similar, the combination of the results of the four experiments increased the statistics by a factor of four. The combination was made for the 2HDM type II and the preliminary 95% exclusion plot is shown in Fig. 6.1. The preliminary lower mass limit for any leptonic branching ratio is $78.6 \text{ GeV}/c^2$. The final combination of the results of the four experiments will be done after all collaborations have published their final results.

6.2 Hadron colliders and indirect searches

The Tevatron collider at Fermilab facilitates the collisions of proton and antiproton beams at the centre-of-mass energy of 1.8 TeV. The two experiments at Tevatron, CDF and D0, have

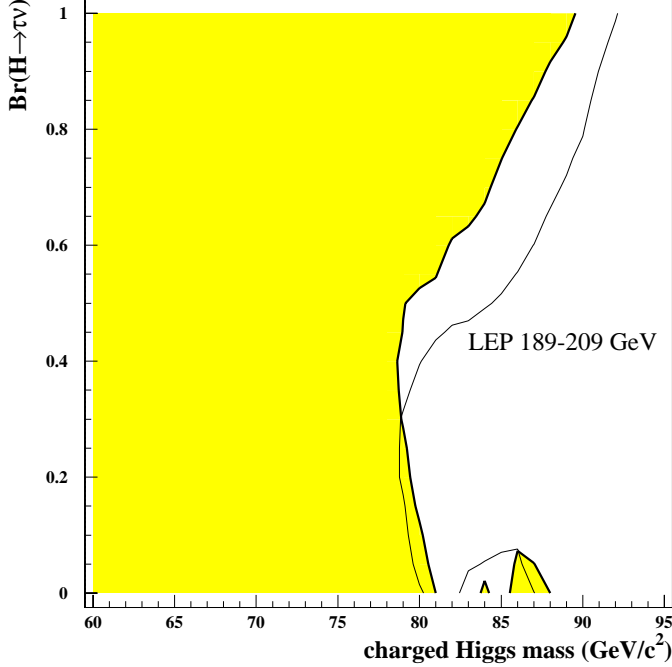


Figure 6.1: Preliminary observed and expected exclusion regions at 95% confidence level in the plane of $\text{Br}(H \rightarrow \tau^- \bar{\nu}_\tau)$ vs. M_{H^\pm} for 2HDM type II. These limits were obtained from a combination of the search results of the four LEP experiments using data collected at $\sqrt{s} = 189\text{--}209$ GeV [34].

searched for charged Higgs bosons in top quark decays looking directly for the $t \rightarrow H^+ b \rightarrow \tau \nu b$ decay process. They have also indirectly excluded some regions of the $[M_{H^+}, \tan\beta]$ plane by using the constraint where they have measured the $t \rightarrow W^+ b$ branching fraction to be above 0.5 (or 0.6), which excludes the large value of the tbH^+ coupling [35, 36, 37].

If a charged Higgs boson existed, its contribution in loop corrections could be measurable in some processes such as the $b \rightarrow s\gamma$ penguin decay. The rate of this process has been measured by the CLEO collaboration at the Cornell Electron Storage Ring (CESR). The result of the measurement is in agreement with the Standard Model and sets the following mass limit for the charged Higgs boson [38]

$$M^{H^\pm} > [244 + 63/(\tan\beta)^{1.3}] \text{GeV}$$

Results of the $b \rightarrow X_s \gamma$ measurements from CLEO, BELLE and ALEPH collaborations have been combined in a recent publication [39] and a $\tan\beta$ independent limit

$$M^{H^\pm} > 315 \text{GeV}$$

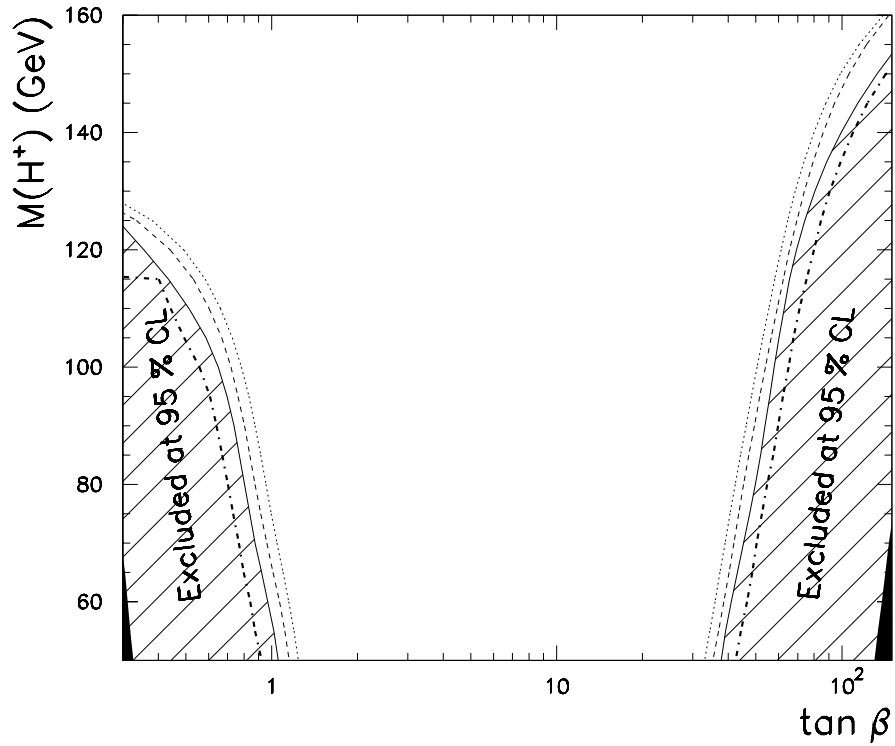


Figure 6.2: Regions of the $[M_{H^+}, \tan\beta]$ plane excluded by the D0 collaboration [35].

has been obtained for 2HDM type II.

These indirect mass limits obtained from loop processes are sensitive to any additional particles in the model. Any new particle which is not included in the present calculation could contribute to the loop process cross-sections and cancel out the contribution of the charged Higgs boson invalidating the mass limit.

Chapter 7

H^+H^- searches in future experiments

No experimental evidence for the existence of charged Higgs bosons and no confirmation whatsoever of the Higgs mechanism have been found so far. LEP has been shut down and the only high energy frontier collider operating now is Tevatron. Tevatron, however, has only limited potential to extend its search for charged Higgs bosons during the second phase of its operation, Run II. The experimental discovery and confirmation of the mass creation mechanism will probably be postponed until the experiments at the Large Hadron Collider (LHC) at CERN start. LHC experiments are expected to be able to discover at least one Higgs boson or to exclude completely the SM and SUSY Higgs mechanisms if nothing is found. The ability of LHC to study the structure and parameters of the Higgs sector are, however, limited. If Higgs bosons exist, a high energy linear e^+e^- collider would be able to determine their properties with higher precision.

7.1 The Large Hadron Collider

The Large Hadron Collider (LHC) is a 14 TeV proton-proton collider expected to start operating at CERN in 2007. The two experiments, ATLAS and CMS, will be able to search for charged Higgs bosons in several different processes. The LHC proton-proton collisions will produce large numbers of t quarks, and a charged Higgs boson with mass less than about $160 \text{ GeV}/c^2$ can be discovered or excluded by the LHC experiments using the $t \rightarrow H^+ \rightarrow \tau\nu$ decay channel [40]. The leptonic decay $H^+ \rightarrow \tau\nu$ can also be used above the t quark mass, where the charged Higgs boson can be produced in the $gb \rightarrow tH^\pm$ process. The leptonic decay channel has sufficient rates with large values of $\tan\beta$ and this channel can be used to discover or exclude the existence of charged Higgs bosons up to masses of several hundreds of GeV/c^2 , with the assumption that $\tan\beta$ is above 10 [41]. The hadronic decay channel $H^+ \rightarrow tb$ has a significant rate for charged Higgs bosons with masses up to about $400 \text{ GeV}/c^2$ with low or high $\tan\beta$ (below 2 or above 20) [42]. Regions of expected 5σ discovery sensitivity in the $[m_{H^\pm}, \tan\beta]$ plane for the ATLAS detector are shown in Fig. 7.1.

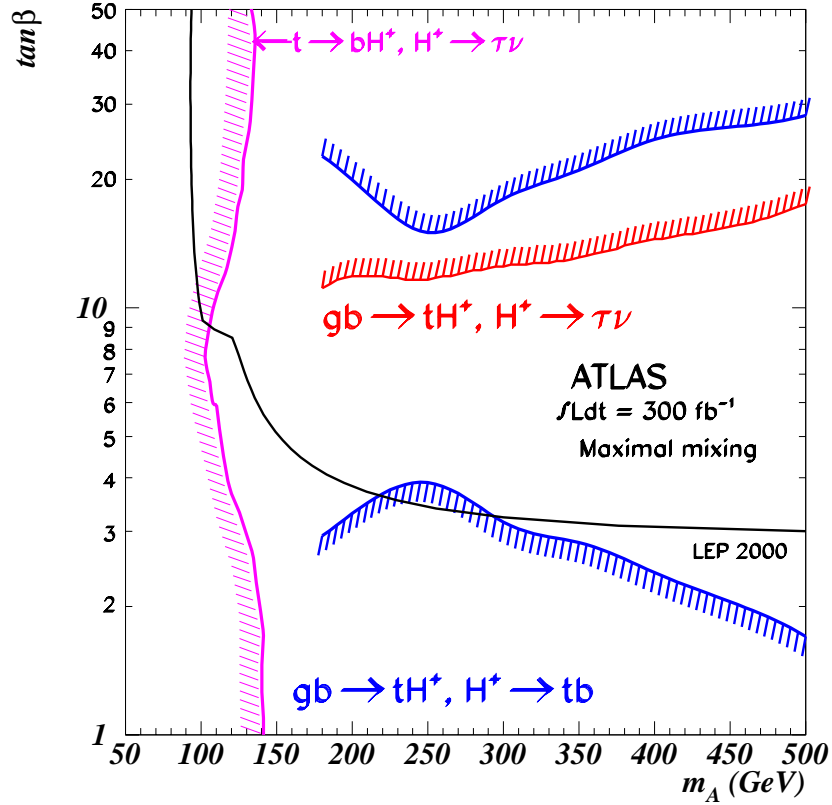


Figure 7.1: Regions of the $[M_{H^+}, \tan \beta]$ plane where the ATLAS experiment is expected to have 5σ sensitivity for charged Higgs bosons [43].

The LHC experiments will not have sensitivity for the charged Higgs boson if $\tan \beta$ has a value in the range from about 5 to 10. The same also holds for other heavier Higgs bosons in this intermediate range of values for $\tan \beta$. The LHC experiments will be able to discover the lightest SM or SUSY Higgs boson at any $\tan \beta$ value, but they may be unable to see any other Higgs bosons, especially if $\tan \beta$ has a moderate value (see Fig. 7.2). In addition, it is possible that the LHC experiments will not be able to measure the properties of a possibly discovered Higgs boson precisely enough to tell which Higgs boson they have found. The discovery potential of the ATLAS experiment for different Higgs bosons is shown in Fig. 7.2.

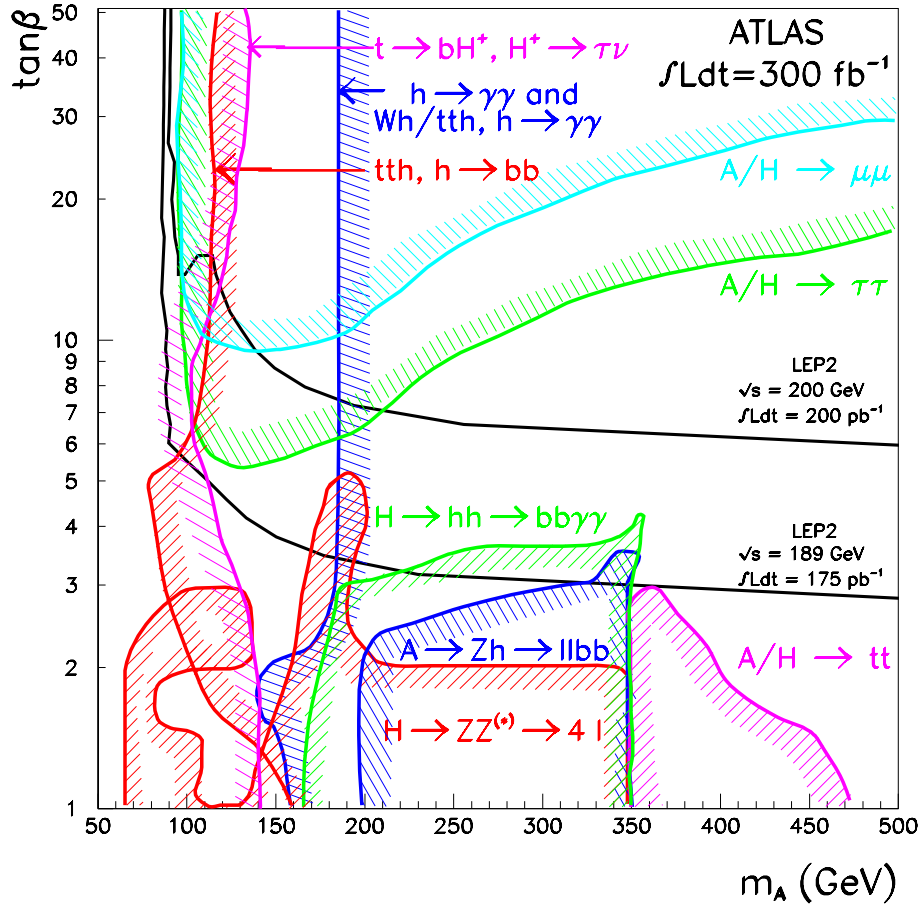


Figure 7.2: Regions of the $[M_H, \tan \beta]$ plane where the ATLAS experiment is expected to have 5σ sensitivity for different kinds of Higgs bosons [44].

7.2 Linear electron positron colliders

There is a wide consensus in the high energy physics community about a linear electron-positron collider being the next major high energy frontier machine after the LHC. An electron-positron collider is needed to complement the physics program of LHC, as many processes can be studied more accurately in a low background environment. Electron-positron colliders above the LEP energy can not be circular storage rings, due to too large synchrotron radiation energy losses, and so a TeV range collider must therefore be linear [45].

The technology for a 500-1000 GeV linear collider exists and there are already proposals to build such a machine so that it could start operating soon after 2010 [46]. There is also ongoing research and development of two-beam acceleration technology for a compact collider with centre-of-mass energy of about 3 TeV [47].

Charged Higgs bosons could be pair-produced in e^+e^- collisions if the mass of the charged

Higgs boson is less than half of the available collision energy. The discovery potential for charged Higgs bosons has been one of the topics of interest as long as the idea of 500-1000 GeV colliders has been under detailed study [48], [49], [50]. These early studies have shown that a charged Higgs boson could be discovered at a high energy linear collider in various decay channels.

Publication VI demonstrates for the first time that it is possible to perform full event reconstruction of the hadronic eight-jet final state of $H^+H^- \rightarrow t\bar{t}b\bar{b}$ decay, which is the dominant decay channel above the t mass threshold in most of the models. It also shows that this reconstruction method works with similar performance for the alternative $H^+H^- \rightarrow W^+h^0W^-h^0$ decay, which has the same eight-jet final state topology as the $H^+H^- \rightarrow t\bar{t}b\bar{b}$ decay. Publication VII contains a further study with more complete background simulations and shows that full reconstruction of all objects in the $H^+H^- \rightarrow t\bar{t}b\bar{b} \rightarrow W^+b\bar{b}W^-b\bar{b} \rightarrow \text{eight jets}$ decay chain allows very efficient reduction of all six and eight fermion backgrounds.

Publication VII shows two reference points: a $300 \text{ GeV}/c^2$ charged Higgs boson at a 800 GeV centre-of-mass energy and a $880 \text{ GeV}/c^2$ charged Higgs boson at a 3 TeV centre-of-mass energy. With the use of kinetic fits, the mass of the charged Higgs boson can be measured accurately, with a relative precision of up to 1%. Fig. 7.3 (from publication VII) shows the reconstructed mass distribution for a simulated $300 \text{ GeV}/c^2$ charged Higgs boson at an 800 GeV e^+e^- collider. The sensitivity of the analyses allows discovery of the Higgs boson signal up to about $350 \text{ GeV}/c^2$ mass at an 800 GeV collider and up to about $1 \text{ TeV}/c^2$ at a 3 TeV collider.

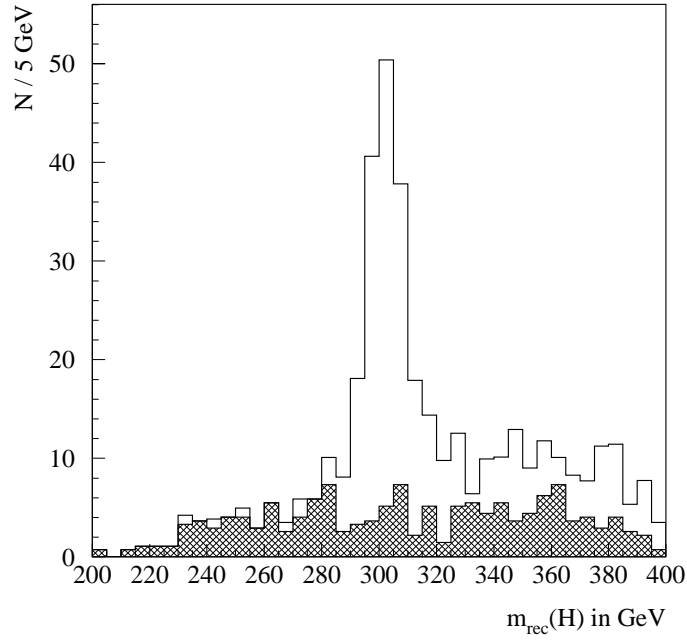


Figure 7.3: Fitted mass of the charged Higgs bosons in $H^+H^- \rightarrow t\bar{t}b\bar{b}$ process with $m_H = 300 \text{ GeV}/c^2$ (open histogram). The contribution of the $t\bar{t}b\bar{b}$ background is shown as a dark histogram. The histograms are normalised to correspond to an integrated luminosity of 1 ab^{-1} at 800 GeV collision energy. A hundred percent branching fraction has been assumed for $H^+H^- \rightarrow t\bar{t}b\bar{b}$.

Chapter 8

Conclusions

The origin of the particle masses is the most burning question to be answered in modern particle physics. The Higgs mechanism provides a solution within the Standard Model. However, no experimental confirmation of the existence of Higgs particles has been found so far.

The Standard Model can not be the final theory of matter and interactions. It is successful in describing the phenomena observed at energies available in the present experiments, but needs to be extended for higher energies.

Theories that go beyond the Standard Model predict the existence of new particles which become important in interactions at higher energies. These theories also contain extensions to the Higgs sector of the Standard Model predicting many kinds of Higgs particles, including charged ones.

Charged Higgs bosons, as predicted by two Higgs doublet models, have been searched for at LEP over a large mass range. No signal has been found and strict lower mass limits have been set with various model assumptions. New methods developed for the LEP charged Higgs boson searches and results of the DELPHI analyses have been presented in this thesis.

Searches for the Higgs bosons will continue in future experiments. Studies presented in this thesis show that a full reconstruction of complicated eight-jet decay processes would be possible at high-energy linear electron-positron colliders. If such a collider is built and if a charged Higgs boson exists within its energy reach, the charged Higgs boson will be discovered and many of its properties will be measured.

References

- [1] Kerson Huang, QUARKS, LEPTONS & GAUGE FIELDS (2nd edition), (World Scientific, 1992).
- [2] F. Halzen and A.D. Martin, QUARKS AND LEPTONS: An Introductory Course in Modern Particle Physics, (John Wiley & Sons, 1984).
- [3] W.N. Cottingham and D.A. Greenwood, An Introduction to the Standard Model of Particle Physics, (Cambridge University Press, 1998).
- [4] Particle Data Group, Eur. Phys. J. **C15** (2000) 1–878.
- [5] Particle Data Group, Phys. Rev. **D66** (2002) 010001.
- [6] Gordon Kane, Modern elementary particle physics: the fundamental particles and forces?, (Addison-Wesley Publishing Company, 1993).
- [7] L. Susskind, Phys. Rept. **104** (1984) 181–193.
- [8] Michael E. Peskin and Daniel V. Schroeder, An Introduction to Quantum Field Theory, (Perseus Books, 1995).
- [9] Byron P. Roe, Particle Physics at the New Millennium, (Springer-Verlag, 1996).
- [10] S. Weinberg, A Unified Physics by 2050?, Scientific American, December 1999 issue.
- [11] John F. Gunion, Howard E. Haber, Gordon Kane and Sally Dawson, The Higgs Hunter's Guide, (Perseus Books, 1990).
- [12] S.L. Glashow and A. Weinberg, Phys. Rev. **D15** (1977) 1958.
- [13] M.Carena, P.M.Zerwas, Higgs Physics, in Physics at LEP2, edited by G.Altarelli, T.Sjostrand and F.Zwirner, CERN Report 96-01, Vol. 1, pages 351-462.
- [14] Y. Grossman, Nucl. Phys. **B426** (1994) 355–384.
- [15] F.M. Borzumati and A. Djouadi, Phys. Lett. **B549** (2002) 170–176.
- [16] A. Djouadi, J. Kalinowski and P.M. Zerwas, Z. Phys. **C70** (1996) 435–448.

- [17] A.G. Akeroyd, Nucl. Phys. **B544** (1999) 557.
- [18] P. Aarnio et al. (DEPHI Collaboration), Nucl. Instr. and Meth. **A303** (1991) 233.
- [19] P. Abreu et al. (DEPHI Collaboration), Nucl. Instr. and Meth. **A378** (1996) 57.
- [20] Ya.I. Azimov, Yu.L. Dokshitzer, V.A. Khoze and S.I. Troyan, Z. Phys. **C27** (1985) 65.
- [21] Ya.I. Azimov, Yu.L. Dokshitzer, V.A. Khoze and S.I. Troyan, Z. Phys. **C31** (1986) 213.
- [22] B.R. Webber, Int. J. Mod. Phys. **A15S1** (2000) 577–606.
- [23] B. Andersson, G. Gustafson, G. Ingelman and T. Sjostrand, Phys. Rep. **97** (1983) 31–145.
- [24] T. Sjostrand, Computer Physics Commun. **82** (1994) 74.
- [25] S. Catani, Yu.L. Dokshitzer, M. Olsson, G. Turnock and B.R. Webber, Phys. Lett. **B269** (1991) 432.
- [26] N. Kjaer and R. Moller, DELPHI 91-17 PHYS 88.
- [27] N. Kjaer, PUFITC program, available from the author.
- [28] P. Abreu et al. (DELPHI Collaboration), Eur. Phys. J. **C2** (1998) 581.
- [29] A.L. Read, Modified Frequentist Analysis of Search Results (the CL_s Method), in CERN Report 2000-005 (2000), p.81.
- [30] R. Barate et al. (ALEPH Collaboration), Phys. Lett. **B543** (2002) 1–13.
- [31] M. Acciarri et al. (L3 Collaboration), Phys. Lett. **B575** (2003) 208–220.
- [32] K. Ackerstaff et al. (OPAL Collaboration), Phys. Lett. **B426** (1998) 180–192.
- [33] OPAL Collaboration, Search for Charged Higgs Bosons in e^+e^- Collisions at $\sqrt{s} = 189 - 209$ GeV, OPAL PHYSICS NOTE PN509, July 18, 2002.
- [34] The LEP Collaborations and the LEP Higgs Working Group, Search for Charged Higgs bosons: Preliminary Combined Results Using LEP Data Collected at Energies up to 209 GeV, LHWG note 2001-05, DELPHI 2001-115 CONF 538 (4 July, 2001).
- [35] B. Abbot et al. (D0 Collaboration), Phys. Rev. Lett. **82** (1999) 4975–4980.
- [36] F. Abe et al. (CDF Collaboration), Phys. Rev. Lett. **79** (1997) 357.
- [37] T. Affolder et al. (CDF Collaboration), Phys. Rev. **D62** (2000) 012004.
- [38] M.S. Alam et al. (CLEO Collaboration), Phys. Rev. Lett. **74** (1995) 2885–2889.
- [39] P. Gambino and M. Misiak, Nucl. Phys. **B611** (2001) 338–366.
- [40] S. Banerjee and M. Maity, J. Phys. G: Nucl. Part. Phys. **28** (2002) 2443–2452.

- [41] K. A. Assamagan and Y. Coadou, *Acta Phys. Polon.* **B33** (2002) 707–720.
- [42] K. A. Assamagan, *Acta Phys. Polon.* **B31** (2000) 863–879.
- [43] K. A. Assamagan, Y. Coadou and A. Deandrea, *Eur. Phys. J. direct* **4** (2002) 9.
- [44] ATLAS collaboration, ATLAS DETECTOR AND PHYSICS PERFORMANCE, Technical Design Report, Volume II, CERN/LHCC 99-15, 1999.
- [45] Edmund Wilson, *An Introduction to Particle Accelerators*, (Oxford University Press, 2001).
- [46] TESLA collaboration, TESLA (The Superconducting Electron-Positron Linear Collider with an Integrated X-Ray Laser Laboratory) Technical Design Report, DESY 2001-011 (2001).
- [47] The CLIC Study Team, A 3 TeV e+e- Linear Collider based on CLIC Technology, CERN 2000-008 (2000).
- [48] S. Komamiya, *Phys. Rev.* **D38** (1988) 2158.
- [49] P. Eerola and J. Sirkka, Charged Higgs Production at High Energy Linear Colliders, DESY 92-123A (1992) 133.
- [50] A. Sopczak, *Z. Phys.* **C65** (1995) 449.